

Renal sodium gradient orchestrates a dynamic antibacterial defence zone

Authors: Miriam R. Berry¹, Rebecca J. Mathews¹, John R. Ferdinand¹, Chenzhi Jing¹, Kevin W. Loudon¹, Elizabeth Wlodek¹, Thomas W. Dennison¹, Christoph Kuper², Wolfgang Neuhofer², Menna R. Clatworthy^{1*}

Affiliations:

¹Molecular Immunity Unit, University of Cambridge Department of Medicine, Cambridge, UK.

² Department of Physiology, University of Munich, D-80336, Munich, Germany

*To whom correspondence should be addressed:

Molecular Immunity Unit

University of Cambridge Department of Medicine

MRC Laboratory of Molecular Biology,

Cambridge Biomedical Campus,

Francis Crick Avenue,

Cambridge. CB2 0QH.

Phone: 44-1223-267279

Email: mrc38@cam.ac.uk

Summary

Lower urinary tract infections are among the commonest human bacterial infections but extension to the kidneys is rare. This has been attributed to mechanical forces, such as urine flow, that prevent the ascent of bladder microbes. Here we show that the regional hypersalinity, required for the kidney's urine-concentrating function, instructs epithelial cells to produce chemokines that localize monocyte-derived mononuclear phagocytes (MNPs) to the medulla. This hypersaline environment also increases the intrinsic bactericidal and neutrophil chemotactic activities of MNPs to generate a zone of defence. Because MNP positioning and function are dynamically regulated by the renal salt gradient, we find that patients with urinary concentrating defects are susceptible to kidney infection. Our work reveals a critical accessory role for the homeostatic function of a vital organ in optimizing tissue defence.

Introduction

Tissue-specific immunity is shaped by the local milieu. In organ systems that interface with the environment, including the skin and gastrointestinal tract, exogenous signals generated by commensal bacteria or diet profoundly influence resident immune cells (Naik et al., 2012) and may even give rise to regional compartmentalization of immune cell subsets (Atarashi et al., 2013; Ivanov et al., 2009). In the gut, microbial cues are also critical for the homeostatic replenishment of resident macrophages from the circulating monocyte pool (Bain et al., 2014). In non-interfacing tissues, endogenous signals such as interstitial osmolality may influence the immune landscape. Indeed, increased extracellular sodium skews CD4 T cells to a Th17 phenotype (Kleinewietfeld et al., 2013; Wu et al., 2013).

Tissue epithelial cells play an important role as environmental sensors and contribute to local immune responses directly or via cross-talk with local immune cells (Machnik et al., 2009; Olszak et al., 2014; Sano et al., 2015; Unkel et al., 2012). In addition, environmental cues may be detected by tissue-resident immune cells, including mononuclear phagocytes (MNPs) (Jantsch et al., 2015; Kinnebrew et al., 2012; Naik et al., 2015). All organs contain a network of MNPs, comprising macrophages and dendritic cells (DCs), poised to respond to local stimuli. Several tissue DC and macrophage subsets have been described in both mice and humans based on surface markers and ontogeny (Guilliams et al., 2014; Varol et al., 2015). In humans, CD11c and MHC class II-positive cells comprise two broad subsets of tissue-resident MNPs, based on the presence or absence of CD14. CD14- cells represent classical myeloid DC (mDC), with the capacity to migrate and present or cross-present antigen, whilst CD14+ cells are macrophage-like with an avid phagocytic capacity (Haniffa et al., 2012; Segura et al., 2012) and arise from circulating monocytes (McGovern et al., 2014).

The mammalian kidney presents a unique environment for resident MNPs, with extreme hypersalinity in the medulla, generated to achieve its homeostatic function of water reabsorption (Koepsell et al., 1974). The kidney is also a dynamic environment, with variation in the magnitude of the intrarenal sodium gradient depending on physiological need. In response to dehydration and elevated serum osmolality, vasopressin secreted by the posterior pituitary generates a further increase in interstitial sodium in the medulla, and promotes the reabsorption of free water, restoring normovolaemia (Knepper et al., 2015; Levitin et al., 1962). The phylogeny of urine concentrating mechanisms is temporally related to the evolution of the urinary bladder (Kondo et al., 2006), which allows for controlled voiding but produces a static fluid collection in which bacteria can multiply and ascend into the kidney. Urinary tract infections (UTIs) are most frequently caused by uropathogenic *Escherichia coli* (UPEC) and represent one of the commonest bacterial infections in humans. Notably, UTIs predominantly

affect the lower urinary tract (Foxman, 2014). This has been attributed to mechanical forces, such as urine flow, that prevent the ascent of microbes from the bladder, but whether additional protective mechanisms operate in the kidney is unknown.

Here we show that in the human kidney, the high interstitial sodium concentration in the medulla generates a defence zone with enhanced antibacterial immunity in the area first encountered by bacteria ascending from the bladder. Medullary hypersalinity provides a cue to renal tubular epithelial cells, causing NFAT5-dependent production of chemokines that orchestrate the recruitment of circulating monocyte-derived MNPs into the region, and this effect is augmented by the presence of *E.coli* lipopolysaccharide (LPS). These CD14⁺ MNPs are adept at phagocytosing UPEC and their bactericidal and neutrophil chemotactic function further increased by hypersalinity. Using mouse models, we show that medullary recruitment of monocyte-derived MNPs is NFAT5 and CCL2-dependent. Finally, we demonstrate the *in vivo* relevance of these observations, where disruption of the renal sodium gradient in patients and mice, leads to aberrant chemokine expression, a reduction in monocyte recruitment and impaired MNP localization to the medulla, and increased susceptibility to pyelonephritis.

This elegant mechanism provides a way to calibrate tissue defence with infectious risk; by utilizing the environmental signal required for urine concentration to generate a defence zone, the immune system reinforces the most vulnerable region of the kidney when it is at greatest risk. During dehydration, the physical conditions favour infection due to reduced urine flow, with less mechanical propulsion of bacteria away from the kidney. Our data suggest that, in just such conditions, the heightened medullary sodium concentration ensures local antibacterial defence is at its most efficient. We therefore reveal a unique mechanism whereby changes in the tissue environment generated by the homeostatic function of the organ stimulate epithelial-MNP cross-talk to optimize tissue defence.

Results

Anti-bacterial CD14⁺ MNPs are enriched in the renal medulla

The mammalian kidney is a unique environment for tissue-resident cells with marked regional differences between the cortex where filtrate is generated, and the medulla where water is reabsorbed. Given data showing the importance of macrophages and DCs in defence against UTI in murine models (Carey et al., 2016; Tittel et al., 2011), we sought to characterize MNPs in the human kidney and to examine whether there were micro-anatomical differences in their distribution. Analysis of human renal tissue revealed CD45⁺/Lineage⁻/CD11c⁺/MHCII^{hi} MNPs by flow cytometry (Figure 1A, B) and confocal microscopy (Figure 1C). This population could be further subdivided into CD14⁺ and CD14⁻ subsets, of which the CD14⁺ subset was the more numerous (Figure 1B) and were CD11b⁺, CD64⁺ and CD68⁻ (Figure S1A), as observed in CD14⁺ MNPs in the skin (McGovern et al. 2014). When comparing samples from cortex and medulla, we observed an enrichment of CD14⁺ cells within the medulla (Figure 1D, E). To ensure that this was not related to differential efficacy of tissue dissociation, we incubated cortical and medullary explants *ex vivo*; significantly more CD14⁺ MNPs migrated from medulla compared with cortex (Figure 1E, S1B). The distribution of CD14⁺ DCs was not impacted by patient age, gender, kidney function or time in cold storage prior to analysis (Figure S1C).

The mammalian kidney is at particular risk from bacteria ascending from the urinary bladder to the medulla and the anatomical location of CD14⁺ MNPs in the human kidney would place them in a prime position to combat such infections. We therefore investigated the efficacy of CD14⁺ MNPs in defence against UPEC, the most common cause of UTI (Foxman, 2014). CD14⁺ MNPs from human kidneys showed significantly greater phagocytosis of fluorescently labelled UPEC compared with CD14⁻ cells and 4°C controls (Figure 1F and Figure S1D,E). They also produced more of the neutrophil-recruiting chemokine IL8 (Figure 1G) in response to UPEC stimulation than CD14⁻ MNPs, and more TNF- α and IL-6 (Figure 1H), both of which have been shown to augment neutrophil responses to UPEC (Godaly et al., 2001; Steadman et al., 1991). Consistent with this, supernatants obtained from medullary cell suspensions stimulated with UPEC enhanced neutrophil phagocytosis and myeloperoxidase secretion compared with cortical supernatants (Figure 1I), an effect to which CD11c⁺ cells substantially contributed (Figure 1J). Together, these data show an enrichment of antibacterial CD14⁺ MNPs in the human renal medulla, that following exposure to UPEC, produce IL8 that can potentially mobilise neutrophils, and neutrophil-activating cytokines to combat ascending infection.

Variation in chemokine expression in different regions of the kidney

Chemokines play a critical role in driving MNP migration and localization (Randolph et al., 2008). We therefore determined whether there was variability in chemokine expression in different regions of the kidney. Transcriptomic analysis of human kidneys showed marked micro-anatomical variation in several chemokines that might influence immune cell positioning (Figure 2A). We further investigated CX3CL1 and CCL2 (MCP1), since these chemokines are known to impact MNP migration (Ancuta et al., 2003; Kuziel et al., 1997). In addition, the receptors for these two chemokines were the only ones expressed to any significant extent on kidney CD14⁺ MNPs (Figure 2B and Fig S2A). We therefore examined CX3CL1 and CCL2 transcript levels in human kidneys by rtPCR and confirmed a 2 to 8 fold increase in the medulla compared with the cortex (Figure 2C). Confocal imaging demonstrated CX3CL1 protein within medullary tubular epithelial cells, at a significantly higher level than that in cortical tubular cells (Figure 2D, E). CCL2 transcripts were also higher in isolated tubular epithelial cell sorted from the medulla compared with the cortex (Figure S2B). To determine the functional significance of these observations, we performed an *ex vivo* migration assay, incubating blocks of human kidney in cell culture medium with or without recombinant CX3CL1 or CCL2. Addition of either chemokine increased migration of CD14⁺ MNPs (Figure 2F-G). These data suggest that local CX3CL1 and CCL2 attract CD14⁺ MNPs to the human renal medulla.

Environmental hypersalinity instructs NFAT5-dependent chemokine secretion by kidney epithelial cells

Given the importance of epithelial cells in sensing environmental cues in non-renal tissues (Machnik et al., 2009; Olszak et al., 2014; Sano et al., 2015; Unkel et al., 2012), we next examined how high extracellular sodium concentration might influence renal tubular epithelial cells. In particular we asked whether a high salt environment might promote their secretion of chemokines. In order to recapitulate the extreme extracellular sodium concentration in the medulla (Gottschalk and Mylle, 1959) (which may vary between 250mmol/L and 400 mmol/L depending on hydration), we cultured a human renal tubular epithelial cell line, HK2, with standard medium (containing 130 mmol/L sodium) supplemented with up to 120 mmol/L of additional sodium chloride. We observed a significant increase in both CCL2 and CX3CL1 in the presence of salt, an effect augmented by the presence of *E. coli* LPS (Figure 3A). The increase in CCL2 and CX3CL1 transcripts and in CCL2 and CX3CL1 secretion was specific to sodium, was not observed when tubular cells were cultured with an osmolar control (mannitol, Figure S3A) and was not associated with an increase in tubular cell death (Figure S3B). HEK293 T cells also produced CCL2 and CX3CL1 in response to increasing extracellular sodium (Figure S3C).

NFAT5 (TonEBP) is a ubiquitous transcription factor that is involved in cellular adaptation to hyperosmolarity (Ho, 2006). In support of a role for this pathway in mediating the effects of

hypersalinity on renal tubular cells, we observed increased expression of *NFAT5*, as well as one of its targets *SLC5A3* (a sodium/myoinositol channel) (Klaus et al., 2008) in the renal medulla compared with the cortex (Figure 3B-D). Furthermore, *NFAT5* knockdown in human kidney epithelial cells significantly attenuated the sodium-dependent increase in chemokine production (Figure 3E and Figure S3D). *NFAT5* activation involves proteasomal processing and phosphorylation by kinases, including p38 MAPK (Kojima et al., 2010), which was also upregulated in the medulla (Figure 3B). Inhibition of the proteasome or p38 function also abrogated salt-dependent chemokine production by renal tubular epithelial cells (Figure 3F), confirming the importance of *NFAT5* in mediating the epithelial cell response to extracellular sodium.

Disruption of the renal sodium gradient leads to aberrant chemokine production and MNP localization

We next sought to determine if changes in the renal sodium gradient would impact chemokine production by epithelial cells and the subsequent localization of CD14⁺ MNPs. As noted previously, vasopressin (anti-diuretic hormone (ADH)) promotes water reabsorption in the kidney and increases the medullary sodium concentration (Levitin et al., 1962). Secretion of vasopressin by the pituitary may be severely impaired in patients with head injury, leading to a failure in urine concentration and subsequent reduction in the renal sodium gradient (Levitin et al., 1962), a condition known as diabetes insipidus (DI). We examined human kidney tissue from patients with DI (Figure S4A) and observed that *NFAT5* was no longer highly expressed in the medulla compared with the cortex (Figure 4A), as we had observed in controls (Figure 3C), confirming a loss of the intrarenal sodium gradient in patients with DI. We also observed a loss of differential expression of *CX3CL1* and *CCL2* between cortex and medulla (Figure 4B and Figure S4B), and fewer CD14⁺ MNPs in the medulla (Figure 4C). Of note, patients with DI were comparable to controls in terms of prior drug therapy, age, gender, kidney function, time in cold storage, co-morbidities, and inflammatory markers (Figure S4C). These data demonstrate that in the absence of medullary hypersalinity, there is a loss of intrarenal chemokine gradient and a reduction in CD14⁺ MNPs in the medulla.

To confirm the importance of the renal sodium gradient in positioning kidney MNPs, we examined mouse kidneys. Using confocal microscopy and flow cytometric analysis, we observed an asymmetrical distribution of MNPs, with more CD11c⁺ cells in the cortex and an enrichment of CD11b^{hi}F4/80⁺ MNPs in the medulla and pelvis (designated MNP2, Figure 4D-F). As in human kidneys, we observed a higher level of *Ccl2* transcripts in the medulla of murine kidneys compared with the cortex (Figure 4G). Although *CX3CL1* is differentially expressed in human kidneys, with high levels in medulla, we did not consider this axis to be of

relevance in murine kidneys since published data demonstrate that CX3CR1⁺ MNPs in mouse kidney are preferentially located in the cortex, and that these cells are dispensable for defence against infection (Hochheiser et al., 2013).

We investigated the impact of medullary hypersalinity on the intrarenal CCL2 gradient and the differential distribution of kidney MNPs by inducing DI in mice using tolvaptan (a vasopressin receptor 2 antagonist (Berl, 2015) or demeclocycline (which reduces vasopressin receptor expression and signaling (Kortenoeven et al., 2013)). This disrupted the cortical location of CD11c⁺ MNPs (Figure S4D,E), led to a reduction in the number of medullary CD11b^{hi}F4/80⁺ MNP2 (Figure 4H) and the abrogation of the intrarenal CCL2 gradient (Figure 4I). Similarly, in neonatal mice, that lack urine concentrating ability (Edwards et al., 1981) CD11c⁺ MNPs were uniformly distributed between the cortex and medulla until 18-24 days of age (Figure S4F). Differential localization of MNPs to the different anatomical compartments within the neonatal kidney occurred in parallel with increasing urine osmolality and sodium (Figure S4G, H). To confirm the importance of the CCL2-CCR2 axis in mediating MNP positioning in the medulla we first neutralized CCL2. This resulted in a loss of the medullary enrichment of CD11b^{hi}F4/80⁺ MNP2 (Figure S4I), as did genetic deletion of CCR2 (Figure 4J, K). We also observed that CD11b^{hi} F4/80⁺ MNP2 were reduced within the medulla of *Nfat5*-deficient mice, (generated by crossing *Nfat5*^{fl/fl} mice with animals with a tamoxifen-inducible derivative of the Cre-recombinase under the control of the *UbiquitinC* promoter, Figure 4L, M) as were renal *Ccl2* transcript levels (Figure S4J). Taken together, the human and mouse data show that the medullary positioning of specific MNP subsets is orchestrated by the regional hypersalinity via NFAT5-dependent production of CCL2.

NFAT5-dependent CCL2 promotes monocyte recruitment to the renal medulla

Ki67 staining of CD11b^{hi}F4/80⁺ MNP2 in the cortex and medulla demonstrated no significant increase in proliferation in medullary positioned cells (Figure S5A). Since CD14⁺ MNP in human skin are thought to be monocyte-derived (McGovern et al., 2014), we sought to determine if circulating monocytes were preferentially recruited into the kidney medulla compared with the cortex, contributing to an enrichment in monocyte-derived MNPs in the medulla. CD45.1 monocytes were transferred intravenously into CD45.2 recipient mice and the kidneys harvested after 6 days (Figure 5A). A higher number of CD45.1⁺ cells were observed in the medulla compared with the cortex, and this differential recruitment was lost in mice with DI, demonstrating the importance of the intra-renal sodium gradient for monocyte recruitment (Figure 5A). To determine whether medullary monocyte recruitment was CCL2-dependent, we administered a CCL2-neutralising antibody prior to monocyte transfer. This led to a reduction in the preferential recruitment of circulating monocytes to the kidney medulla (Figure 5B). To

confirm the importance of the CCL2-CCR2 axis in monocyte recruitment to the medulla, we transferred congenically marked WT and *Ccr2*-deficient monocytes into a WT recipient and after 1 week, assessed medullary monocyte-derived cells (Figure 5C). This demonstrated an enrichment of WT monocyte-derived cells in the medulla, but few *Ccr2*-deficient cells in medulla (Figure 5D-E). We next assessed the impact of *Nfat5* deficiency on kidney chemokine production and monocyte recruitment using *Nfat5^{fl/fl} Ert2-Cre* mice (Figure 5F). Fourteen days following the initial administration of tamoxifen, we observed a variable but significant reduction in *Nfat5* transcripts in the kidney (Figure S5B) but a striking correlation between *Nfat5* and *Ccl2* levels (Figure 5G). In keeping with this, there was a significant reduction in the recruitment of congenically marked WT monocytes to the kidneys of tamoxifen-treated *Nfat5^{fl/fl} Ert2-Cre* mice (Figure 5H). Together, these data suggest that the high sodium concentration in the renal medulla stimulates NFAT5-dependent production of CCL2 that acts to recruit circulating monocytes into the region in a CCR2-dependent manner, and that this preferential recruitment contributes to the medullary positioning of MNP2.

Medullary hypersalinity enhances the anti-bacterial function of CD14+ MNPs

Since tissue specific environmental cues can directly impact resident MNPs (Jantsch et al., 2015; Kinnebrew et al., 2012; Naik et al., 2015) and immune cell function may be significantly influenced by extracellular sodium concentration (Ip and Medzhitov, 2015; Jantsch et al., 2015; Junger et al., 1994; Kleinewietfeld et al., 2013; Shapiro and Dinarello, 1995; Wu et al., 2013; Zhang et al., 2015), we asked whether the high salt environment of the medulla might enhance CD14+ MNP function. When comparing cortical and medullary CD14+ MNPs, we observed increased phagocytosis of UPEC and IL8 production in medullary MNPs (Figure 6A-B). *In vitro*, increasing extracellular sodium resulted in enhanced UPEC phagocytosis, bacterial killing and cytokine production in human (Figure 6C-F and Figure S6A) and murine MNPs (Figure S6B, C) and this was dependent on NFAT5 (Figure 6G). Furthermore, extracellular hypersalinity also improved the sentinel function of MNPs, leading to enhanced “seek behaviour” with more active dendrite extension and a greater area of scanning in MNPs incubated with high salt (Figure 6H). These data show that the high medullary sodium generates a zone that not only attracts MNPs specialized in antibacterial defence, but also augments their function.

Loss of intrarenal sodium gradient results in susceptibility to pyelonephritis

Given the impact of the high sodium environment of the renal medulla on MNP localization *in vivo*, and on their antibacterial function *in vitro*, we hypothesized that disruption of the renal sodium gradient would impair the medullary defence zone and increase susceptibility to pyelonephritis. Mice treated with tolvaptan or demeclocycline for 7 days to induce DI had significantly higher bacterial load, neutrophil infiltration and abscess formation within the kidney

following intravesical challenge with UPEC (Figure 7A, B and Figure S7A-B). Importantly, this pharmacological abrogation of the renal sodium gradient also resulted in a higher incidence of bacteraemia and death (Figure 7C).

The induction of DI resulted in the loss of the intrarenal CCL2 gradient (Figure 4I) and a reduction in the localization of monocyte-derived MNPs to the medulla (Figure 4H). To assess the importance of CCL2-dependent positioning of medullary MNPs in defence against urosepsis we treated mice with a CCL2-neutralising antibody for 6 days prior to induction of UTI. This resulted in increased severity of infection (Figure 7D). Similarly *Ccr2*-deficient mice also had more severe infection following UPEC challenge (Figure 7E).

We had observed that NFAT5 was required for salt-dependent chemokine production by human renal tubular cells *in vitro* (Figure 3A) and the medullary recruitment of monocyte-derived MNPs *in vivo* (Figure 4L and 5E). We therefore asked whether NFAT5-dependent processes were important in defence against kidney infection *in vivo*. We observed an inverse correlation between kidney *Nfat5* levels and the number of kidney CFUs cultured from the kidneys of mice with DI following UPEC challenge (Figure 7F). To confirm the importance of NFAT5 on the outcome of UTI *in vivo*, we treated mice with lithium, which is known to reduce NFAT5 protein expression in kidney tubular cells in hyperosmolar conditions and cause DI (Kuper et al., 2015). Mice with a lithium-induced reduction in renal *Nfat5* expression (Figure S7C) demonstrated worse outcomes following UPEC challenge, with increased pyelonephritis, bacteraemia and death (Figure 7G). Similarly, tamoxifen-treated *Nfat5^{fl/fl} Ert2-cre* mice also had increased pyelonephritis and kidney CFUs compared with controls (Figure 7H)

In humans, pharmacological induction of DI with tolvaptan has been used to slow cyst growth in Autosomal Dominant Polycystic Kidney Disease (ADPKD) (Higashihara et al., 2011). A dose-dependent increase in the frequency of UTI was observed in patients with ADPKD treated with tolvaptan (Higashihara et al., 2011) (Figure 7I). We next investigated the incidence of UTI in patients with sickle cell disease (SCD), where thrombosis of the medullary vasa recta results in an inability to maintain a renal sodium gradient or concentrate urine (Hatch et al., 1967; Stadius van Eps et al., 1970). Our meta-analysis showed an increased frequency of UTIs in SCD patients compared with controls (Figure 7J and Figure S7D). Finally, in organ donors with DI (in which we had shown a reduction in medullary *NFAT5*, *CX3CL1* and *CCL2* expression, and in the number of CD14⁺ MNPs, Figure 4A-D) there was an increased frequency of bacterial growth from protocol ureteric cultures compared with non-DI donors (Figure 7K and Figure S7E), despite the fact that high urine flow is thought to protect from UTI by promoting the physical expulsion of bacteria away from the kidney. Thus, in a murine model of UTI and in

patients with ADPKD, pharmacological disruption of the sodium gradient increases susceptibility to infection. Similarly, in patients with pathological disruption of the sodium gradient due to nephrogenic (SCD) or cranial (organ donors) DI, an increased frequency of UTI was observed.

Discussion

Tissue-specific cues orchestrate the anatomical position of resident immune cells, to optimize function. To date, this paradigm has been best described in organ systems interfacing with the environment, such as skin or the gastrointestinal tract, where colonizing commensal bacteria provide signals to orientate immune cells and compartmentalize immune responses. In the skin, DCs localize to commensal-rich appendages such as hair follicles, from where they may be able to directly sample microbial products (Naik et al., 2015; Naik et al., 2012). In the gut, regional differences in the type of local commensal leads to an expansion of T-helper-17 cells (Th17) or regulatory T cell populations within the ileum and colon respectively (Atarashi et al., 2013; Ivanov et al., 2009). The microbiota is also required for the constant recruitment of intestinal macrophages from circulating monocytes (Bain et al., 2014). Here we describe how the extreme electrolyte concentration generated within a micro-anatomical region of the kidney, is similarly used to recruit and compartmentalize functionally-specialized MNPs to the renal medulla.

Although epithelial cells are not conventionally considered to be immune effectors, there is increasing evidence that they are important tissue sensors that can be influenced by environmental cues to have direct immune activity (Olszak et al., 2014) and to communicate with local immune cells. Such communication may optimize immune cell function, for example, in the ileum, epithelial production of serum amyloid A induces IL17A expression in Th17 cells (Sano et al., 2015). Alternatively, epithelial cells may dictate immune cell localization; in the murine lung, alveolar epithelial cells secrete GM-CSF that is required for the homeostatic presence of CD103⁺ DCs in the lung parenchyma and for the recruitment of CD11b⁺ and monocyte-derived DCs during infection (Unkel et al., 2012). Here we identify epithelial:MNP cross-talk in the human kidney, whereby tubular epithelial cells orchestrate the recruitment of monocyte-derived CD14⁺ MNPs to the medulla via the production of CCL2. This mirrors the homeostatic replenishment of intestinal macrophages from the circulating monocyte pool that is microbiota-dependent (Bain et al., 2014). However, in the kidney, the local environmental signal is interstitial sodium rather than a microbial cue. The fact that chemokine production can be further augmented by exposure to *E. coli* LPS supports the importance of kidney epithelial cells in generating a dynamic medullary defence zone, and controlling its magnitude in-line with concurrent immunological information.

Although, in addition to CCL2, we also observed an increase in CX3CL1 expression and CD14⁺CX3CR1⁺ MNPs in human kidney medulla, and in HK2 cells cultured with increasing sodium, we did not interrogate this axis in mice because previous studies have shown that CX3CR1⁺ MNPs in the mouse kidney are enriched in the cortex rather than the medulla

(Hochheiser et al., 2013). This demonstrates that the precise chemokines that determine MNP localization in the kidney in human and mouse may differ and illustrates that mouse models do not always provide a read-out relevant to the human. Furthermore, although HK2 cells are a human renal proximal tubular cell line rather than primary human tubular epithelial cells, with the known limitations of cell lines, none the less, the data generated support the importance of extracellular sodium concentration and NFAT5 in driving differences in chemokine expression observed between cortex and medulla.

A number of reports suggest that extracellular sodium may impact immune cell function. In the adaptive immune system, an increase in extracellular sodium of 40 mmol/L above baseline can augment the induction of Th17 cells and the suppressive capacity of regulatory T cells (Hernandez et al., 2015; Kleinewietfeld et al., 2013; Wu et al., 2013). In MNPs high salt may increase macrophage cytokine production *in vitro* (Ip and Medzhitov, 2015; Junger et al., 1994; Shapiro and Dinarello, 1995; Zhang et al., 2015), as well as the response of skin macrophages to the protozoan parasite *Leishmania in vivo* (Jantsch et al., 2015). The medulla of the kidney is an extreme hypersaline environment (Gottschalk and Mylle, 1959) for immune cells, with extracellular sodium concentrations far higher than those described in lymphoid tissue or skin (Jantsch et al., 2015). We demonstrate that in this zone of hypersalinity the antibacterial function of local MNPs is enhanced, with increased UPEC phagocytosis, bacterial killing and cytokine production, including the neutrophil chemoattractant IL8 (CXCL8). The latter is of particular significance in the context of UTI, since neutrophils are recruited to the kidney during ascending infection (Godaly et al., 2001) and this is critical for effective defence, as evidenced by studies demonstrating that polymorphisms in the IL8 and IL8 receptor genes are associated with increased susceptibility to pyelonephritis (Artifoni et al., 2007; Lundstedt et al., 2007). Mice lack IL8, but express analogous chemokines that ligate CXCR2, including CXCL2 (MIP-2), and mediate neutrophil recruitment. *Cxcr2*-deficient mice are susceptible to severe pyelonephritis and even develop renal abscesses (Svensson et al., 2008). Notably, we demonstrated enhanced CXCL2 production by murine MNPs in the presence of high salt (Figure S6C).

The kidney not only constitutes an environment with marked regional differences, but is also a highly dynamic environment for tissue-resident cells. The magnitude of the intrarenal sodium gradient varies significantly depending on hydration status. During dehydration, the relative sodium concentration within the renal medulla increases to facilitate water reabsorption from filtrate to concentrate urine and restore normovolaemia. This scenario produces physical conditions that are permissive for infection, with low urine flow and reduced expulsion of bacteria ascending from the bladder. Our data suggest that it is in just such conditions that the medullary defence zone is optimized. This is achieved by utilizing the same environmental

signal that is required for urine concentration to position antibacterial MNPs in the medulla and to augment their function. This elegant mechanism allows local conditions to orchestrate a responsive and adaptable defence zone, commensurate with the likely challenge; when physical expulsion of bacteria is at its weakest, tissue-resident sentinels are strengthened by the local hypersalinity. These findings also have important clinical implications, suggesting that the current practice of increasing fluid intake during UTIs may be counter-productive, due to the negative impact of reduced medullary sodium on the position and anti-bacterial function of local MNPs.

In summary, our work elucidates the mechanisms mediating effective tissue-specific immunity within the kidney, and reveals a critical accessory role for the homeostatic function of a vital organ in optimizing local defence to protect it from bacterial invaders.

Author contributions:

MB, RM and JF designed and performed experiments, and co-wrote the methods and figure legends. CJ, KL, TD and EW performed experiments. CK and WN provided reagents/experimental animals. MRC conceived the project, designed and performed experiments and wrote the manuscript.

Acknowledgements:

MRB is supported by a Medical Research Council/Kidney Research UK Research Training Fellowship (MR/K023934/1) and previously The Evelyn Trust Clinical Research Fellowship. CJ is funded by the China Scholarship Council (No. 201408060241). RJM and MRC are supported by the National Institute of Health Research (NIHR) Cambridge Biomedical Research Centre, MRC and JRF by the NIHR Blood and Transplant Research Unit and MRC by a Medical Research Council New Investigator Research Grant (MR/N024907/1). The Molecular Immunity Unit is within the MRC Laboratory of Molecular Biology and the authors are grateful for the use of the core facilities.

We thank: Professor Lalita Ramakrishnan, Dr Ronald Germain, Professor Kenneth Smith, Professor Paul Edelstein and Mr Steven Levitte for helpful discussions: Dr Edward Banham-Hall, Mr Keith Burling, Professor Donald Fraser, Mr Michael Hope, Dr Robert Jenkins, Dr Darren Roberts, Dr David Thomas and Dr Patrick Trotter for technical advice and assistance:

Dr Antonio Bravo-Blas and Dr Elizabeth Mann for sharing murine tissue, Dr Callum Bain and Prof Simon Jenkins for the kind gift of the CCR2^{-/-} mice, the NIHR Cambridge BRC Cell Phenotyping Hub: The Evelyn Trust: Mr Marcus Gregson: NHS Blood and Transplant and all transplant co-ordinators, organ donors and their families.

References:

- Ancuta, P., Rao, R., Moses, A., Mehle, A., Shaw, S.K., Luscinikas, F.W., and Gabuzda, D. (2003). Fractalkine preferentially mediates arrest and migration of CD16+ monocytes. *J Exp Med* 197, 1701-1707.
- Artifoni, L., Negrisolo, S., Montini, G., Zucchetto, P., Molinari, P.P., Cassar, W., Destro, R., Anglani, F., Rigamonti, W., Zacchello, G., *et al.* (2007). Interleukin-8 and CXCR1 receptor functional polymorphisms and susceptibility to acute pyelonephritis. *J Urol* 177, 1102-1106.
- Atarashi, K., Tanoue, T., Oshima, K., Suda, W., Nagano, Y., Nishikawa, H., Fukuda, S., Saito, T., Narushima, S., Hase, K., *et al.* (2013). Treg induction by a rationally selected mixture of Clostridia strains from the human microbiota. *Nature* 500, 232-236.
- Bain, C.C., Bravo-Blas, A., Scott, C.L., Gomez Perdiguero, E., Geissmann, F., Henri, S., Malissen, B., Osborne, L.C., Artis, D., and Mowat, A.M. (2014). Constant replenishment from circulating monocytes maintains the macrophage pool in the intestine of adult mice. *Nat Immunol* 15, 929-937.
- Berl, T. (2015). Vasopressin Antagonists. *N Engl J Med* 373, 981.
- Boring, L., Gosling, J., Chensue, S.W., Kunkel, S.L., Farese, R.V., Jr., Broxmeyer, H.E., and Charo, I.F. (1997). Impaired monocyte migration and reduced type 1 (Th1) cytokine responses in C-C chemokine receptor 2 knockout mice. *J Clin Invest* 100, 2552-2561.
- Carey, A.J., Sullivan, M.J., Duell, B.L., Crossman, D.K., Chattopadhyay, D., Brooks, A.J., Tan, C.K., Crowley, M., Sweet, M.J., Schembri, M.A., *et al.* (2016). Uropathogenic Escherichia coli Engages CD14-Dependent Signaling to Enable Bladder-Macrophage-Dependent Control of Acute Urinary Tract Infection. *J Infect Dis* 213, 659-668.
- Edwards, B.R., Mendel, D.B., LaRoche, F.T., Stern, P., and Valtin, H. (1981). Postnatal development of urinary concentrating ability in rats: changes in renal anatomy and neurophysial hormones. In *The kidney during development: morphology and function*, A. Spitzer, ed. (New York: Masson), pp. 233-240.
- Foxman, B. (2014). Urinary tract infection syndromes: occurrence, recurrence, bacteriology, risk factors, and disease burden. *Infectious disease clinics of North America* 28, 1-13.
- Gentleman, R.C., Carey, V.J., Bates, D.M., Bolstad, B., Dettling, M., Dudoit, S., Ellis, B., Gautier, L., Ge, Y., Gentry, J., *et al.* (2004). Bioconductor: open software development for computational biology and bioinformatics. *Genome biology* 5, R80.
- Godaly, G., Bergsten, G., Hang, L., Fischer, H., Frendeus, B., Lundstedt, A.C., Samuelsson, M., Samuelsson, P., and Svanborg, C. (2001). Neutrophil recruitment, chemokine receptors, and resistance to mucosal infection. *J Leukoc Biol* 69, 899-906.
- Gottschalk, C.W., and Mylle, M. (1959). Micropuncture study of the mammalian urinary concentrating mechanism: evidence for the countercurrent hypothesis. *Am J Physiol* 196, 927-936.
- Guilliams, M., Ginhoux, F., Jakubzick, C., Naik, S.H., Onai, N., Schraml, B.U., Segura, E., Tussiwand, R., and Yona, S. (2014). Dendritic cells, monocytes and macrophages: a unified nomenclature based on ontogeny. *Nat Rev Immunol* 14, 571-578.
- Haniffa, M., Shin, A., Bigley, V., McGovern, N., Teo, P., See, P., Wasan, P.S., Wang, X.N., Malinarich, F., Malleret, B., *et al.* (2012). Human Tissues Contain CD141(hi) Cross-Presenting Dendritic Cells with Functional Homology to Mouse CD103(+) Nonlymphoid Dendritic Cells. *Immunity* 37, 60-73.
- Hatch, F.E., Culbertson, J.W., and Diggs, L.W. (1967). Nature of the renal concentrating defect in sickle cell disease. *J Clin Invest* 46, 336-345.
- Hernandez, A.L., Kitz, A., Wu, C., Lowther, D.E., Rodriguez, D.M., Vudattu, N., Deng, S., Herold, K.C., Kuchroo, V.K., Kleinewietfeld, M., *et al.* (2015). Sodium chloride inhibits the suppressive function of FOXP3+ regulatory T cells. *J Clin Invest* 125, 4212-4222.

Higashihara, E., Torres, V.E., Chapman, A.B., Grantham, J.J., Bae, K., Watnick, T.J., Horie, S., Nutahara, K., Ouyang, J., Krasa, H.B., *et al.* (2011). Tolvaptan in autosomal dominant polycystic kidney disease: three years' experience. *Clinical journal of the American Society of Nephrology : CJASN* 6, 2499-2507.

Higgins, J.P., Wang, L., Kambham, N., Montgomery, K., Mason, V., Vogelmann, S.U., Lemley, K.V., Brown, P.O., Brooks, J.D., and van de Rijn, M. (2004). Gene expression in the normal adult human kidney assessed by complementary DNA microarray. *Mol Biol Cell* 15, 649-656.

Ho, S.N. (2006). Intracellular water homeostasis and the mammalian cellular osmotic stress response. *Journal of cellular physiology* 206, 9-15.

Hochheiser, K., Heuser, C., Krause, T.A., Teteris, S., Ilias, A., Weisheit, C., Hoss, F., Tittel, A.P., Knolle, P.A., Panzer, U., *et al.* (2013). Exclusive CX3CR1 dependence of kidney DCs impacts glomerulonephritis progression. *J Clin Invest* 123, 4242-4254.

Hung, C.S., Dodson, K.W., and Hultgren, S.J. (2009). A murine model of urinary tract infection. *Nat Protoc* 4, 1230-1243.

Ip, W.K., and Medzhitov, R. (2015). Macrophages monitor tissue osmolarity and induce inflammatory response through NLRP3 and NLRC4 inflammasome activation. *Nature communications* 6, 6931.

Ivanov, I.I., Atarashi, K., Manel, N., Brodie, E.L., Shima, T., Karaoz, U., Wei, D., Goldfarb, K.C., Santee, C.A., Lynch, S.V., *et al.* (2009). Induction of intestinal Th17 cells by segmented filamentous bacteria. *Cell* 139, 485-498.

Jantsch, J., Schatz, V., Friedrich, D., Schroder, A., Kopp, C., Siegert, I., Maronna, A., Wendelborn, D., Linz, P., Binger, K.J., *et al.* (2015). Cutaneous Na⁺ storage strengthens the antimicrobial barrier function of the skin and boosts macrophage-driven host defense. *Cell metabolism* 21, 493-501.

Junger, W.G., Liu, F.C., Loomis, W.H., and Hoyt, D.B. (1994). Hypertonic saline enhances cellular immune function. *Circulatory shock* 42, 190-196.

Kinnebrew, M.A., Buffie, C.G., Diehl, G.E., Zenewicz, L.A., Leiner, I., Hohl, T.M., Flavell, R.A., Littman, D.R., and Pamer, E.G. (2012). Interleukin 23 production by intestinal CD103⁺CD11b⁺ dendritic cells in response to bacterial flagellin enhances mucosal innate immune defense. *Immunity* 36, 276-287.

Klaus, F., Palmada, M., Lindner, R., Laufer, J., Jeyaraj, S., Lang, F., and Boehmer, C. (2008). Up-regulation of hypertonicity-activated myo-inositol transporter SMIT1 by the cell volume-sensitive protein kinase SGK1. *J Physiol* 586, 1539-1547.

Kleinewietfeld, M., Manzel, A., Titze, J., Kvakana, H., Yosef, N., Linker, R.A., Muller, D.N., and Hafler, D.A. (2013). Sodium chloride drives autoimmune disease by the induction of pathogenic TH17 cells. *Nature* 496, 518-522.

Knepper, M.A., Kwon, T.H., and Nielsen, S. (2015). *Molecular Physiology of Water Balance*. *N Engl J Med* 373, 196.

Koepsell, H., Nicholson, W.A., Kriz, W., and Hohling, H.J. (1974). Measurements of exponential gradients of sodium and chlorine in the rat kidney medulla using the electron microprobe. *Pflugers Arch* 350, 167-184.

Kojima, R., Taniguchi, H., Tsuzuki, A., Nakamura, K., Sakakura, Y., and Ito, M. (2010). Hypertonicity-induced expression of monocyte chemoattractant protein-1 through a novel cis-acting element and MAPK signaling pathways. *J Immunol* 184, 5253-5262.

Kondo, Y., Morimoto, T., Nishio, T., Aslanova, U.F., Nishino, M., Farajov, E.I., Sugawara, N., Kumagai, N., Ohsaga, A., Maruyama, Y., *et al.* (2006). Phylogenetic, ontogenetic, and pathological aspects of the urine-concentrating mechanism. *Clin Exp Nephrol* 10, 165-174.

Kortenoeven, M.L., Sinke, A.P., Hadrup, N., Trimpert, C., Wetzels, J.F., Fenton, R.A., and Deen, P.M. (2013). Demeclocycline attenuates hyponatremia by reducing aquaporin-2 expression in the renal inner medulla. *Am J Physiol Renal Physiol* 305, F1705-1718.

Kuper, C., Beck, F.X., and Neuhofer, W. (2014). Generation of a conditional knockout allele for the NFAT5 gene in mice. *Front Physiol* 5, 507.

Kuper, C., Beck, F.X., and Neuhofer, W. (2015). Dual effect of lithium on NFAT5 activity in kidney cells. *Front Physiol* 6, 264.

Kuziel, W.A., Morgan, S.J., Dawson, T.C., Griffin, S., Smithies, O., Ley, K., and Maeda, N. (1997). Severe reduction in leukocyte adhesion and monocyte extravasation in mice deficient in CC chemokine receptor 2. *Proc Natl Acad Sci U S A* 94, 12053-12058.

Levitin, H., Goodman, A., Pigeon, G., and Epstein, F.H. (1962). Composition of the renal medulla during water diuresis. *J Clin Invest* 41, 1145-1151.

Lindquist, R.L., Shakhar, G., Dudziak, D., Wardemann, H., Eisenreich, T., Dustin, M.L., and Nussenzweig, M.C. (2004). Visualizing dendritic cell networks in vivo. *Nat Immunol* 5, 1243-1250.

Lundstedt, A.C., McCarthy, S., Gustafsson, M.C., Godaly, G., Jodal, U., Karpman, D., Leijonhufvud, I., Linden, C., Martinell, J., Ragnarsdottir, B., *et al.* (2007). A genetic basis of susceptibility to acute pyelonephritis. *PLoS One* 2, e825.

Machnik, A., Neuhofer, W., Jantsch, J., Dahlmann, A., Tammela, T., Machura, K., Park, J.K., Beck, F.X., Muller, D.N., Derer, W., *et al.* (2009). Macrophages regulate salt-dependent volume and blood pressure by a vascular endothelial growth factor-C-dependent buffering mechanism. *Nat Med* 15, 545-552.

McGovern, N., Schlitzer, A., Gunawan, M., Jardine, L., Shin, A., Poyner, E., Green, K., Dickinson, R., Wang, X.N., Low, D., *et al.* (2014). Human dermal CD14(+) cells are a transient population of monocyte-derived macrophages. *Immunity* 41, 465-477.

Naik, S., Bouladoux, N., Linehan, J.L., Han, S.J., Harrison, O.J., Wilhelm, C., Conlan, S., Himmelfarb, S., Byrd, A.L., Deming, C., *et al.* (2015). Commensal-dendritic-cell interaction specifies a unique protective skin immune signature. *Nature* 520, 104-108.

Naik, S., Bouladoux, N., Wilhelm, C., Molloy, M.J., Salcedo, R., Kastenmuller, W., Deming, C., Quinones, M., Koo, L., Conlan, S., *et al.* (2012). Compartmentalized control of skin immunity by resident commensals. *Science* 337, 1115-1119.

Olszak, T., Neves, J.F., Dowds, C.M., Baker, K., Glickman, J., Davidson, N.O., Lin, C.S., Jobin, C., Brand, S., Sotlar, K., *et al.* (2014). Protective mucosal immunity mediated by epithelial CD1d and IL-10. *Nature* 509, 497-502.

Randolph, G.J., Ochando, J., and Partida-Sanchez, S. (2008). Migration of dendritic cell subsets and their precursors. *Annu Rev Immunol* 26, 293-316.

Sano, T., Huang, W., Hall, J.A., Yang, Y., Chen, A., Gavzy, S.J., Lee, J.Y., Ziel, J.W., Miraldi, E.R., Domingos, A.I., *et al.* (2015). An IL-23R/IL-22 Circuit Regulates Epithelial Serum Amyloid A to Promote Local Effector Th17 Responses. *Cell* 163, 381-393.

Schaefer, B.C., Schaefer, M.L., Kappler, J.W., Marrack, P., and Kiedl, R.M. (2001). Observation of antigen-dependent CD8+ T-cell/ dendritic cell interactions in vivo. *Cell Immunol* 214, 110-122.

Schmittgen, T.D., and Livak, K.J. (2008). Analyzing real-time PCR data by the comparative C(T) method. *Nat Protoc* 3, 1101-1108.

Segura, E., Valladeau-Guilemond, J., Donnadieu, M.H., Sastre-Garau, X., Soumelis, V., and Amigorena, S. (2012). Characterization of resident and migratory dendritic cells in human lymph nodes. *J Exp Med* 209, 653-660.

Shapiro, L., and Dinarello, C.A. (1995). Osmotic regulation of cytokine synthesis in vitro. *Proc Natl Acad Sci U S A* 92, 12230-12234.

- Stadius van Eps, L.W., Pinedo-Veels, C., de Vries, G.H., and de Koning, J. (1970). Nature of concentrating defect in sickle-cell nephropathy. *Microradiangiographic studies. Lancet* 1, 450-452.
- Steadman, R., Matthews, N., Lichodziejewska, M., and Williams, J.D. (1991). Human neutrophil responses to pathogenic *Escherichia coli* are receptor-specific and selectively augmented by recombinant human tumor necrosis factor- α . *J Infect Dis* 163, 1033-1039.
- Svensson, M., Irljala, H., Svanborg, C., and Godaly, G. (2008). Effects of epithelial and neutrophil CXCR2 on innate immunity and resistance to kidney infection. *Kidney Int* 74, 81-90.
- Tittel, A.P., Heuser, C., Ohliger, C., Knolle, P.A., Engel, D.R., and Kurts, C. (2011). Kidney dendritic cells induce innate immunity against bacterial pyelonephritis. *J Am Soc Nephrol* 22, 1435-1441.
- Unkel, B., Hoegner, K., Clausen, B.E., Lewe-Schlosser, P., Bodner, J., Gattenloehner, S., Janssen, H., Seeger, W., Lohmeyer, J., and Herold, S. (2012). Alveolar epithelial cells orchestrate DC function in murine viral pneumonia. *J Clin Invest* 122, 3652-3664.
- Varol, C., Mildner, A., and Jung, S. (2015). Macrophages: development and tissue specialization. *Annu Rev Immunol* 33, 643-675.
- Wu, C., Yosef, N., Thalhamer, T., Zhu, C., Xiao, S., Kishi, Y., Regev, A., and Kuchroo, V.K. (2013). Induction of pathogenic TH17 cells by inducible salt-sensing kinase SGK1. *Nature* 496, 513-517.
- Zhang, W.C., Zheng, X.J., Du, L.J., Sun, J.Y., Shen, Z.X., Shi, C., Sun, S., Zhang, Z., Chen, X.Q., Qin, M., *et al.* (2015). High salt primes a specific activation state of macrophages, M(Na). *Cell Res* 25, 893-910.

Figures

Figure 1: Tissue resident macrophages are enriched in the human renal medulla and have enhanced anti-bacterial function

(A-B) Representative FACS plots (A) and quantification of relative frequency (B) of human kidney MNPs demonstrating CD45⁺, CD3/19/15⁻, MHCII^{hi} CD11c^{hi} CD14⁺ and CD14⁻ subsets. Graph shows mean and standard error of mean (SEM) of n=5 human kidneys.

(C) Confocal microscopy of human kidney showing MHC II (green) and CD14 (cyan)⁺ cells within the interstitium (actin, red). Lower power image shown in left panel (scale bar = 100µm). Area in white box magnified and shown in middle panel (scale bar = 20 µm). Area in white box magnified and shown in two right-hand panels.

(D-E) Schematic and representative FACS plots (D) and quantification of CD14⁺ macrophages in human medulla=M and cortex=C, in digested kidney tissue and in cells that migrate from kidney tissue blocks (E). Graphs show mean and SEM of values obtained from n=5 kidney samples.

(F) Representative flow cytometric histogram and quantification of % cells that have phagocytosed UPEC and the MFI of cells in human kidney CD14⁻ (blue) and CD14⁺ (red) MNPs. Graphs show mean and SEM of values obtained from n=5 technical replicates, representative of n=3 independent experiments.

(G) Quantification of IL8 present in culture supernatants obtained from sorted CD14⁻ (black) and CD14⁺ (white) human kidney MNPs incubated with UPEC. Graphs show mean and SEM of values obtained from n=4 technical replicates of n=1 human kidney sample.

(H) Intracellular FACS staining for TNF-alpha and IL6 in CD14⁻ (black) and CD14⁺ (white) human kidney MNPs incubated with UPEC. Each point represents a sample from one kidney.

(I) Neutrophil activating effect of supernatants obtained from kidney cortex (black) and medulla (white) cells following incubation with UPEC: Neutrophil phagocytosis of UPEC (% left and MFI middle) and myeloperoxidase production (right). Graphs show mean and SEM of 4 technical replicates and are representative of results obtained in n=5 kidneys.

(J) Depletion of CD11c⁺ cells from medullary kidney samples reduces neutrophil activating effects of supernatant, as indicated by myeloperoxidase production. Graphs show mean and SEM of 4 technical replicates and are representative of results obtained in n=2 kidneys.

* p<0.05, ** p<0.01, *** p<0.001 and **** p<0.0001 by Student's unpaired (B, I, J) and paired (E-H) t tests.

See also Figure S1.

Figure 2: Chemokine expression in the human kidney

- (A) Heatmap of relative gene expression of selected chemokine transcripts in n=4 paired human cortex and medulla samples. RNA transcripts assessed by microarray and data analyzed with R.
- (B) Representative FACS histograms of CX3CR1 and CCR2 surface expression on CD14⁻ (blue) and CD14⁺ (red) human renal MNPs.
- (C) RT-PCR of *CX3CL1* (left) and *CCL2* (right) mRNA in human kidney cortex and medulla. Data expressed as $2^{-\Delta CT}$.
- (D) Confocal microscopy of CX3CL1 (magenta) staining in human cortex (top panel) and medulla (middle panel). Isotype control staining of medulla section shown in lower panel. Phalloidin staining (white) allows identification of renal tubules. Scale bar -80 μ M.
- (E) Quantification of fluorescence intensity of CX3CL1 staining in cortex and medulla samples. Data obtained from n=5 areas of cortical and medullary renal tubules (t) and interstium (i) and expressed relative to the staining in the tubular isotype control.
- (F-G) Quantification of migration of human renal CD14⁺ (red) and CD14⁻ (blue) MNPs from tissue explants incubated in normal media (Control) or media supplemented with human CCL2 and CX3CL1. Graphs show mean and SEM of n=6 technical replicates, representative of 3 independent experiments.

* p<0.05 and Student's paired (B) and unpaired (E) t tests.

See also Figure S2.

Figure 3: Chemokine secretion by renal tubular epithelium in high salt conditions is NFAT5-dependent

- (A) Quantification of CCL2 (left) and CX3CL1 (right) in supernatants obtained from HK2 cells cultured with increasing concentrations of sodium (black line) + LPS (red line).
- (B) Heatmap of relative gene expression of *NFAT5*, *SLC5A3*, *MAPK13* and *SGK1* in n=4 paired cortex and medulla samples obtained from human kidneys. RNA transcripts assessed by microarray and data analyzed with R.
- (C) RT-PCR of *NFAT5* mRNA in human kidney cortex (blue circles) and medulla (red circles). Data expressed as $2^{-\Delta CT}$.
- (D) Western Blot of NFAT5 protein in human renal cortex and medulla relative to actin.
- (E) Quantification of CCL2 and CX3CL1 in supernatants obtained from HK2 cells cultured with increasing concentrations of salt and control siRNA (black line) or NFAT5 siRNA (red line).

(F) Quantification of CCL2 and CX3CL1 in supernatants obtained from HK2 cells cultured with increasing concentrations of salt (black line) with a p38 inhibitor (red line) or bortezomib (blue line).

** $p < 0.01$ and **** $p < 0.0001$ by paired Student's t test (C) and 2-way ANOVA (A, E, F). For A, E, and F, each square or circle shows the mean and SEM of 3 technical replicates and graphs show representative data from $n=3$ experiments.

See also Figure S3.

Figure 4: Disruption of renal sodium gradient, CCL2-CCR2 axis and NFAT5 causes aberrant chemokine production and MNP positioning

(A-B) Relative mRNA expression of *NFAT5* (A) and *CCL2/CX3CL1* (B) relative in human kidney cortex and medulla obtained from donors with diabetes insipidus (DI, blue boxes) compared with non-DI donors (red boxes). Data expressed as $2^{-\Delta\Delta CT}$. $N > 10$ in each group.

(C) Ratio of CD14+ MNP in human kidney cortex and medulla in donors with DI (blue circles) and controls (red circles). Mean and SEM of all samples shown with horizontal line and error bars respectively.

(D) Confocal imaging of a kidney section obtained from a CD11c eYFP (green) mouse stained with F4/80 (red). Cortex and medulla identified. Low magnification image shown on left (scale bar = $300\mu\text{m}$). High magnification images shown on right (scale bar = $50\mu\text{m}$).

(E) Representative FACS plot and schematic to demonstrate two major populations of CD45+ Lin- F4/80+ MNPs in murine kidney, designated MNP1 and MNP2. Lower panel shows FACS histograms of CD11c expression on these populations.

(F-G) Quantification of MNP2 (F) and relative *Ccl2* mRNA expression (G) in cortex (C) and medulla (M) of control mice.

(H-I) Quantification of MNP2 (H) and relative *Ccl2* mRNA expression (I) in cortex (C) and medulla (M) of Diabetes Insipidus (DI) mice.

(J-K) Quantification (J) and representative FACS plot (K) of MNP in renal medulla of wild-type and *Ccr2*^{-/-} mice.

(L-M) Quantification (L) and representative FACS plot (M) of MNP in renal medulla of *Nfat5*^{fl/fl} and *Nfat5*^{fl/fl} *Ert2-Cre* mice following tamoxifen treatment.

In J and L, each circle represents data from one mouse kidney. Mean and SEM of all samples shown with horizontal line and error bars respectively.

* $p < 0.05$, ** $p < 0.01$, *** $p < 0.001$, **** $p < 0.0001$, NS $p > 0.05$ by unpaired (A-C, J, L) and paired (F-I) Student's t-test.

See also Figure S4.

Figure 5: High interstitial sodium, CCL-CCR2 axis and NFAT5 are required for recruitment of circulating monocytes into renal medulla

- (A) Effect of host Diabetes Insipidus on recruitment of circulating monocytes into renal cortex and medulla. Upper panel - Schematic showing experimental set-up. CD45.2 WT mice treated with tolvaptan (TOL) to induce DI. 6 days later, CD45.1 monocytes transferred IV. Lower panel - Quantification of interstitial CD45.1+ MNP in kidney cortex (blue circle) and medulla (red circle).
- (B) Effect of CCL2 neutralisation on recruitment of circulating monocytes into renal cortex and medulla. Upper panel - Schematic showing experimental set-up. CD45.2 WT mice treated with CCL2 antibody or isotype control antibody. 6 days later, CD45.1 monocytes transferred IV. Lower panel - Quantification of interstitial CD45.1+ MNP in kidney cortex (blue circle) and medulla (red circle).
- (C-E) *Ccr2*-deficient (CD45.2) and WT (CD45.2) monocytes transferred intravenously into a CD45.1/2 mouse. Experimental schematic (C), representative FACS plots (D) and quantification of interstitial CD45.1+ MNP in kidney cortex (blue circle) and medulla (red circle).
- (F-H) *Nfat5^{fl/fl}* or *Nfat5^{fl/fl} Ert2-Cre* CD45.2 mice treated with tamoxifen 7 days prior to intravenous transfer of WT CD45.1 monocytes. Schematic of experimental setup (F) and relationship between *Nfat5* and *Ccl2* expression (G) and recruitment of CD45.1+ cells to the interstitium (H) in the kidneys of *Nfat5^{fl/fl}* (black squares) or *Nfat5^{fl/fl} Ert2-Cre* (Green diamonds) mice. Each point represents a kidney samples. Mean and SEM of all samples shown with horizontal line and error bars respectively.

* $p < 0.05$, ** $p < 0.01$, *** $p < 0.001$ and NS $p > 0.05$ by paired (E) and unpaired (A, B, E, H, J) Student's t tests and linear regression analysis (G).

See also Figure S5.

Figure 6: Medullary hypersalinity enhances antibacterial function of renal macrophages

- (A-B) UPEC phagocytosis (% and MFI) and IL8 production by human cortex and medulla macrophages. Graphs show mean and SEM of $n=5$ technical replicates, representative of $n=3$ independent experiments.
- (C) UPEC phagocytosis (% (left) and MFI (right)) by human monocyte derived macrophage (hMDM) cultured in normal medium (Control, black bars) or medium supplemented with 100 mM additional NaCl (+Na, white bars). Graphs show mean and SEM of 4 technical replicates, representative of 3 independent experiments.

(D) Confocal microscopy of UPEC phagocytosis by human MDMs in normal media (left two panels) and high salt conditions (+100mM Na, right two panels). Actin = white, DAPI = blue, UPEC = green. Scale bar = 10 μ M.

(E) Bacterial (UPEC) killing in hMDM cultured in normal medium (Control, black bars) or with the addition of 100 mM Na (+Na, white bars); propidium iodide+ bacteria (left) and bacterial growth (right). Graphs show mean and SEM of n=3 technical replicates, representative of n=4 independent experiments.

(F) Quantification of IL8, TNF-alpha and IL6 in supernatants obtained from hMDM cultured with UPEC in normal medium (black bars) or with additional Na (white bars). Graphs show mean and SEM of n=6 technical replicates, representative of n=3 independent experiments.

(G) Quantification of UPEC phagocytosis and IL8, TNF-alpha and IL6 production by hMDMs cultured in increasing concentrations of Na following treatment with control siRNA (black line) or NFAT5 siRNA (red line). Graphs show mean and SEM of n=6 technical replicates, representative of n=3 independent experiments.

(H) Representative confocal microscopy images of murine Ubi-GFP BM derived macrophages in normal media (Control, left upper panel) or media with additional 100mmol/L Na (+Na, left lower panel), scale bar =50 μ M, and quantification of surface area during live imaging (right panel) of Ubi-GFP BM derived macrophages in control (black circles) and high salt (red squares) conditions. Each point represents surface area data (mean and SEM) from one cell imaged every 40 seconds over one hour.

* p<0.05, ** p<0.01, *** p<0.001 and **** p<0.0001 by paired (A-B) and unpaired (C-E, G) Student's t test and 2-way ANOVA (F).

See also Figure S6.

Figure 7: Loss of intrarenal sodium gradient confers susceptibility to pyelonephritis

(A) Quantification of bacterial load in renal parenchyma of control (red) and DI (blue) mice. Pooled data from 3 individual experiments.

(B) Confocal images of a kidney obtained from a mouse with DI post-intravesical UPEC challenge. Actin (grey) delineates renal parenchyma. Low power image shown in left panel. White Scale bar = 100 μ M High power magnification of area indicated by red square demonstrates an abscess containing Gr1+ (magenta) neutrophils, CD64+ (blue) MNP and UPEC (green).

(C) Frequency of sepsis events (pyelonephritis, bacteremia or death) in control (red) and diabetes insipidus (blue) mice.

- (D) Frequency of sepsis events (pyelonephritis, bacteraemia or death) in CCL2 Ab treated mice following induction of UTI.
- (E) Frequency of sepsis events (pyelonephritis, bacteraemia or death) (left panel) and bacterial burden (right panel) in WT (red bar) and CCR2^{-/-} mice (blue bar) following induction of UTI.
- (F) Quantification of bacterial load and Nfat5 mRNA expression in kidneys of UTI mice.
- (G) Effect of lithium treatment on frequency of sepsis events (pyelonephritis, bacteraemia and death) in UTI mice.
- (H) Frequency of pyelonephritis (left panel) and bacterial burden (right panel) in WT (red bar) and *Nfat5^{fl/fl} Ert2-Cre* (blue bar) mice following induction of UTI. N=11 mice total.
- (I) Frequency of UTI in Autosomal Dominant Polycystic Kidney Disease patients treated with tolvaptan.
- (J) Meta-analysis of incidence of asymptomatic bacteriuria, UTI and pyelonephritis in patients with sickle cell disease (SCD).
- (K) Effect of donor DI on frequency of ureteric infection in kidney donors.

*p<0.05, ** p<0.01, **** p<0.0001 by unpaired (B, F) Student's t test, linear regression analysis (G) and Chi-squared test (D, E, F, H, K). Bar graphs show mean and SEM.

See also Figure S7.

Supplementary Figure Legends

Figure S1 (related to Figure 1):

- (A) Cell surface staining for macrophage and DC markers in human kidney MNPs.
- (B) Number of CD14+ MNPs that migrated from each gram of cortex and medulla tissue.
- (C) Demographic data of organ donors and effect of donor variables on distribution of CD14+ renal macrophages.
- (D) Confocal microscopy of UPEC phagocytosis and cell surface binding in human MDMs at 4°C and 37°C. Actin = white, DAPI =blue, UPEC = green, UPEC/actin co-localisation = magenta.
- (E) Effect of temperature on fluorescence intensity (MFI) of human kidney MNPs and neutrophils incubated with fluorescent UPEC.

NS $p > 0.05$ by unpaired Student's t-test or linear regression analysis. *** $p < 0.001$, **** $p < 0.0001$ by Student's unpaired t-tests.

Figure S2 (related to Figure 2):

- (A) Cell surface staining for chemokine receptors in human renal MNPs.
- (B) *CCL2* transcript levels in flow sorted CD45-, CD31- tubular epithelial cells obtained from human cortex and medulla samples.

* $p < 0.05$ by paired Student's t-test.

Figure S3 (related to Figure 3):

- (A) Effect of mannitol and salt on HK2 cell *NFAT5* expression and chemokine transcription and production.
- (B) Effect of salt on HK2 cell viability
- (C) Chemokine response of HEK 293T cells to high salt environment.
- (D) Effect of *NFAT5* siRNA on HK2 cell *NFAT5* transcription and production.

* $p < 0.05$, *** $p < 0.001$, **** $p < 0.0001$ by 1-way or 2-way ANOVA, NS $p > 0.05$ by 1-way ANOVA.

Figure S4 (related to Figure 4):

- (A) Urine output and serum sodium in organ donors. Donors with urine output > 4 L/day = DI, < 2.25 L/day = control.
- (B) Relative expression of chemokines in renal cortex and medulla from control and Diabetes Insipidus (DI) donors. Data expressed as $2^{-\Delta CT}$.
- (C) Correlations between donor variables and DI status.

- (D) Confocal microscopy of CD11c eYFP kidneys in control and DI mice. Red=actin, white=CD11c.
- (E) Distribution of CD11c+ kidney cells in adult, neonate and DI mice.
- (F) Confocal microscopy of CD11c eYFP kidneys in adult, day 0.5 and day 6.5 mice (left). Red=actin, white=CD11c.
- (G) Changes in urine osmolality, urine sodium and distribution of CD11c+ cells in neonatal mice (right).
- (H) Correlation between urine osmolality and distribution of CD11c+ cells in mice.
- (I) Effect of CCL2 Ab treatment on frequency of macrophages in renal cortex and medulla.
- (J) Effect of *in vivo* *Nfat5* knockdown on renal expression of *Ccl2*.

*p<0.05 ** p<0.01 *** p<0.001 **** p<0.0001 by unpaired Student's t-test, 2-way ANOVA or linear regression, NS p>0.05 by unpaired Student's t-test or Chi-Squared test.

Figure S5 (related to Figure 5):

- (A) Ki67 expression in murine kidney mononuclear phagocytes in cortex (C) and medulla (M).
- (B) *Nfat5* expression in tamoxifen treated *Nfat^{fl/fl}* (white) and *Nfat5^{fl/fl} Ert2-CRE* (green) mice.

NS p>0.05 by paired Student's t-test, ** p<0.01 by unpaired Student's t-test.

Figure S6 (related to Figure 6):

- (A) Effect of temperature on fluorescence intensity (MFI) of hMDMs incubated with fluorescent UPEC (left). Representative flow cytometry plots of propidium iodide staining of UPEC following intracellular ingestion by hMDMs with/without salt (right).
- (B) UPEC phagocytosis, intracellular CXCL2 staining and TNF α production by murine bone marrow-derived macrophages cultured in salt.

* p<0.05, ** p<0.01, *** p<0.001, p<0.0001 by unpaired Student's t-tests compared to no salt control.

Figure S7 (related to Figure 7):

- (A) Effect of experimental DI on urine and serum osmolality, weight, renal *Nfat5* expression and circulating neutrophil count.
- (B) Effect of DI on kidney-resident neutrophils in UTI mice (left) and confocal microscopy of kidney from control UTI mice. Actin = grey. Gr1= magenta. UPEC=green. CD64=blue.

- (C) Effect of lithium treatment on renal *Nfat5* expression in mice.
- (D) Bibliography for sickle cell disease meta-analysis
- (E) Urine output in organ donors with sterile and positive ureter cultures (left) and methodology for organ donor study (right).

* $p < 0.05$, ** $p < 0.01$, **** $p < 0.0001$, NS $p > 0.05$ by unpaired Student's t-tests.

STAR methods

Contact for reagent and resource sharing

Further information and requests for resources and reagents should be directed to and will be fulfilled by the Lead Contact Menna Clatworthy (mrc38@cam.ac.uk)

MTAs were obtained for the use of NFAT5 fl/fl and NFAT5 fl/fl Ert2-CRE mice between the University of Cambridge and the University of Heidelberg.

Experimental model and subject details

Human subjects

Human kidney samples

Kidneys donated for transplantation, but unsuitable for implantation (due to damage to the arterial patch, parenchymal sclerosis, or suspicion of donor malignancy (Figure S1C) were used. All analysis of human material was performed in the UK; ethical approval was granted by the local ethics committee (REC12/EE/0446) and the study was also approved by NHS Blood and Transplant (NHSBT). Kidneys had a cold ischemic time of less than 30 hours (median 17 hours) prior to processing. Demographic donor data was retrieved from the NHSBT Electronic Offering System (EOS) files (Figure S1C). “Diseased” kidneys were those declined on the basis of abnormal biopsy rather than anatomical or systemic concerns.

Animals

Mice

Wild-type C57BL/6 and UBI-GFP-BL/6 (Schaefer et al., 2001) mice were obtained from Jackson Laboratories Laboratories (Margate, UK). Transgenic mice expressing Venus EYFP under the control of the CD11c promoter (Lindquist et al., 2004) were a gift from M. Nussenzweig (Rockefeller University, New York, USA). *Ccr2*^{-/-} mice (Boring et al., 1997) were a gift from Callum Bain and Simon Jenkins (University of Edinburgh). *Nfat5*^{fl/fl} mice and mice with a tamoxifen-inducible derivative of the Cre-recombinase under the control of the ubiquitinC promoter were gifted by Christoph Kuper and Wolfgang Neuhofer (Kuper et al., 2014). Mice were maintained in specific-pathogen-free conditions at a Home Office-approved facility in the UK. All mice were females aged 6-10 weeks old, weighing 20-25g, group-housed, having undergone no previous procedures. Littermates of the same sex were randomly assigned to different experimental groups. All procedures were conducted in accordance with the United Kingdom Animals (Scientific Procedures) Act 1986.

Cell Lines

Renal tubular epithelial cell culture

HK2 cells (ATCC, Virginia, USA) were cultured to a 60-80% confluent monolayer in a 1:1 mix of DMEM:F12 media containing 2 mM L-Glutamine, 20 mM HEPES, 5 µg/ml transferrin, 5 ng/ml sodium selenite, 400 ng/ml hydrocortisone, supplemented with 10% heat inactivated FCS (all Sigma-Aldrich, Gillingham, UK). Culture medium was supplemented with 0-120 mmol/L sodium chloride (South Devon Healthcare, Torbay, Devon), 0-200 mOsmol/kg 20% mannitol (Baxter, Thetford, UK), 100 ng/ml *E. coli* lipopolysaccharide (Sigma-Aldrich, Gillingham, UK), 10^{-6} M p38i inhibitor SB203580 (Cell Signaling Technology, Danvers, USA), 10^{-9} M bortezomib (SelleckChem, Houston, USA) or DMSO control (Sigma-Aldrich, Gillingham, UK). After 48 hr, supernatants were harvested and CX3CL1 and CCL2 quantified with Quantikine ELISA kits (R and D, Abingdon, UK). Cell viability was assessed using live/dead cell staining (Live/Dead Aqua 405, Invitrogen, Paisley, UK).

Uropathogenic *E. coli* (UPEC)

UPEC (UT189, a gift from S. Hultgren (Hung et al., 2009) in the mid to late log phase of growth were labelled with eFluor 670 (Invitrogen, Paisley UK) for 45 minutes at 37°C, washed with heat-inactivated FCS (Sigma-Aldrich, Gillingham, UK), heat-inactivated at 56°C for 30 minutes and washed 3 times in PBS.

Method details

MNP isolation from human kidneys

Around 30g of kidney tissue was minced and digested in 2.5mg/ml DNase I, 5mg/ml collagenase A and 50mg/ml Dispase II (all Roche, Burgess Hill, UK) in RPMI supplemented with 2% heat inactivated fetal calf serum (FCS) and 1% penicillin-streptomycin (both Sigma-Aldrich, Gillingham, UK), hereafter referred to as complete RPMI. Tissue was dissociated using a Gentle-MACS machine (Miltenyi Biotech, Bisleigh, UK) then passed sequentially through 100 µm, 50 µm and 30 µm cell strainers before density centrifugation using a 44% Percoll (GE Healthcare Life Sciences, Little Chalfont, UK) gradient.

Characterisation of murine kidney MNPs

Immediately following terminal procedure mouse kidneys were perfused with PBS. Organs were dissected into cortex and medulla and minced through a 40 µm cell strainer, digested in 1mg/ml collagenase A, 1mg/ml DNase I (both Roche, Burgess Hill, UK) and 2% heat

inactivated FCS (Sigma-Aldrich, Gillingham, UK) in PBS for 20 minutes, before RBC lysis and filtration through a 30 µm strainer.

Flow cytometry and cell sorting

Cells were blocked with human FcR block (Miltenyi Biotech, Bisley, UK) or normal mouse serum and incubated with antibodies (see Resources Table) for 1 hour at 4°C, followed by live/dead cell staining (Live/Dead Aqua 405, Invitrogen, Paisley, UK) for 20 minutes at room temperature. Cell surface receptor staining was undertaken at room temperature. Intracellular staining was performed using the FoxP3 intracellular staining kit (eBioscience, Hatfield, UK).

Samples were processed on a Fortessa flow cytometer (Becton Dickinson, Basel, Switzerland) and data analyzed using Flowjo software (Treestar, Ashland, TN). Cell sorting was performed on an Aria-Fusion III machine (Becton Dickinson, Basel, Switzerland).

Antibodies (Resource Table) were used at 1 in 100 dilution for flow cytometry. Secondary antibodies were used at 1 in 300 dilution where required.

Immunofluorescence Staining

Samples were fixed in 1% paraformaldehyde (Electron Microscopy Services) / L-lysine/ sodium periodate (both Sigma-Aldrich, Gillingham, UK) buffer for 24 hours followed by 24 hours in 30% sucrose in P-buffer. 20 µm sections were permeabilized and blocked in 0.1M TRIS, containing 0.1% Triton (Sigma), 10% normal mouse serum, 1% BSA (R and D, Abingdon, UK). Images were acquired using an LSM 710 (Carl Zeiss, Cambridge, UK) or TCS SP8 (Leica, Milton Keynes, UK) confocal microscope. Raw imaging data were processed and quantified using Imaris (Bitplane, Zurich, Switzerland). For quantification of tubular and interstitial CX3CL1 staining, a region of interest was manually created over a tubule or area of interstitium using the phalloidin staining to identify these anatomical areas. The mean fluorescence intensity of the CX3CL1 channel was then measured in that region.

Antibodies (Resource Table) were used at 1 in 100 dilution for immunofluorescence.

Secondary antibodies were used at 1 in 300 dilution where required.

Human kidney MNP migration studies

2cm³ tissue samples (approx. 2g) from renal cortex or medulla were incubated at 37°C in complete RPMI overnight. Recombinant human chemokines were added at: 500ng/ml CX3CL1 (Life Technologies, Paisley, UK) and 40ng/ml CCL2 (R and D, Abingdon, UK). Migrated cells present in the well were harvested, washed in cold PBS, stained and analysed by flow cytometry.

UPEC Phagocytosis assay

Fluorescent UPEC were cultured with renal cell suspensions at 37°C for 4-6 hours, in RPMI with 10% FCS (both Sigma-Aldrich, Gillingham, UK). Control wells were incubated at 4°C to adjust for non-specific binding. Following incubation, cells were washed 3 times with cold PBS and processed for flow cytometric analysis.

Neutrophil phagocytosis and myeloperoxidase assay

Fresh human kidney cell suspensions were incubated at 37°C overnight with heat inactivated UPEC. Supernatants were harvested and frozen at -20°C until used. 50ml whole blood was taken from healthy volunteers (Ethical Approval REC 08/H0308/176) and added to 5ml 4% citrate (Sigma-Aldrich, Gillingham, UK). Cell layers were separated with Histopaque 1077 (Sigma-Aldrich, Gillingham, UK) and the granulocyte fraction isolated. Red cells were lysed and remaining cells washed and counted. Human granulocytes were cultured with fluorescent UPEC (+/- kidney supernatant) at 37°C for 60 minutes, with control wells incubated at 4°C to adjust for non-specific binding. Supernatant was retrieved for myeloperoxidase ELISA (R&D Systems, Abingdon UK). Cells were then stained and analyzed by flow cytometry.

CD11c depletion of human renal cell suspensions

Fresh cell suspensions of human renal cortex and medulla were blocked with human FcR block (Miltenyi Biotech, Bisley, UK) and incubated with CD11c beads (BD Biosciences, Oxford, UK) for 20 minutes and washed. Cell suspensions were then passed through LS MACS column (Miltenyi Biotech, Bisley, UK) in the presence of a magnetic field. Depletion was confirmed using flow cytometry.

Reverse Transcriptase Polymerase Chain Reaction

Tissue sections or cell suspensions were lysed in Trizol (Life Technologies, Paisley, UK) and density centrifugation performed using chloroform (Sigma-Aldrich, Gillingham, UK). Subsequent RNA extraction was performed using Ambion RNA PureLink Kit (Life Technologies, Paisley, UK) and yields analyzed using Nanodrop spectrophotometry (Thermo-Scientific, Loughborough, UK). Complementary DNA synthesis was undertaken using High Capacity RNA to cDNA (Life Technologies, Paisley, UK) and BioRad (Hemel Hempstead, UK) PCR machine. RT-PCR was performed using Taqman reagents (Thermo-Fisher, Paisley, UK) on the Viia 7 PCR machine (Life Technologies, Paisley, UK). For primers see Resource Table. Gene expression relative to *GAPDH/HPRT* or *GUSB* calculated using $2^{-\Delta\text{CT}}$ for cortex and medulla individually and $2^{-\Delta\Delta\text{CT}}$ comparatively (Schmittgen and Livak, 2008).

Western Blotting

Nuclear protein lysates of human renal cortex and medulla were prepared using RIPA buffer (Thermo Fisher Scientific, Paisley, UK). 10µg samples were loaded onto a 4-12% Bis-TRIS protein gel (Nupage Novex, Life Technologies, Paisley, UK) at 165V for 45 mins in MOPS-SDS buffer (Thermo Fisher Scientific, Paisley, UK). The gel was then transferred to a nitrocellulose membrane (iBlot Western Blotting System, Invitrogen, Paisely, UK) and blocked for 1 hour at room temperature in 2.5% milk /TBS. The membrane was incubated with primary antibody at 4°C overnight and secondary antibody at room temperature for 2 hours then washed in 2.5% milk/ TBS-Tween. The blot was developed with the LI-COR Odyssey CLx Imager (LI-COR Biosciences – GmbH, UK). Images were quantified using Fiji/ ImageJ software (Bethesda, USA).

For Western Blotting, antibodies (Resources table) were used at 1:1000-1:5000 (primary) and 1:10,000 (secondary) dilution.

NFAT5 knockdown

Lipid complexes of siRNA (using Lipofectamine and Silencer Select siRNA, both Thermo-Fisher, Paisley, UK) were incubated at room temperature for 20 minutes then added to either HK2 cells cultured in OptiMEM (Thermo-Fisher, Paisley, UK) or to human monocyte derived macrophages in serum and antibiotic free RPMI (Sigma-Aldrich, Gillingham, UK). 6 hours later, human monocyte derived macrophages were supplemented with an equal volume of RPMI containing 10% heat inactivated FCS (Sigma-Aldrich, Gillingham, UK). Knockdown efficacy was evaluated using RT-PCR and intracellular staining for NFAT5.

In vivo induction of diabetes insipidus, CCL2 blockade and lithium treatment

Wild-type C57/Bl6 or CD11c eYFP mice were treated with: i) intra-peritoneal demeclocycline 90mg/kg (LKT Laboratories, St Paul, USA), tolvaptan 5 mg/kg (Sigma-Aldrich, Gillingham, UK) or PBS control 12 hourly for 4 days, ii) intra-peritoneal anti-CCL2 antibody 1mg/kg or isotype (both eBiosciences, Hatfield, UK) every 48-72 hr for 10 days, iii) intra-peritoneal lithium chloride 40mg/kg (Sigma-Aldrich, Gillingham, UK) or PBS control daily for 4 days. Animals had free access to drinking water. Biochemical analysis of urine and serum was undertaken at the Core Biochemical Analysis Laboratory in Addenbrooke's Hospital, Cambridge, UK.

In vivo knockdown of Nfat5

Nfat5^{fl/fl} and *Nfat5^{fl/fl} Ert2-Cre* mice were treated daily with 1mg intra-peritoneal tamoxifen (Sigma-Aldrich, Gillingham, UK) on days 0-1 (Fig 4) or days 0-5 (Figure 5, Figure 7H). *Nfat5*

knockdown was subsequently confirmed with RT-PCR. Monocytes were transferred on day 7 (see below) or mice were catheterized and UPEC distilled into the bladder for the UTI model.

Adoptive transfer of monocytes

Femora from wild type, *Ccr2*^{-/-} or *Nfat5*^{fl/fl} *Ert2-Cre* mice were flushed with sterile PBS. Bone marrow monocytes were isolated by negative selection using magnetic cell sorting (Miltenyi Biotech, Surrey, UK) and $0.5 - 1.0 \times 10^6$ cells were transferred into recipient mice via tail vein injection. After 6-7 days recipient mice received 1 μ g intravenous CD45 fluorescent antibody to label circulating cells. Mice were sacrificed, kidneys retrieved and processed in order to identify tissue-resident monocyte derived cells.

Murine bone marrow derived macrophage culture

Femora from wild type or UBI-GFP/BL6 mice were flushed with sterile PBS. Unselected bone marrow cells were incubated in complete RPMI with 0.1 mcg/ml MCSF (Peprotech, London, UK) and supplemented every 72 hours for 5-7 days to culture bone marrow derived monocytes.

Macrophage morphology

Bone marrow derived macrophages were cultured from UBI-GFP/BL6 mice. At day 7, cells were resuspended in PureCol EZ Gel solution (Sigma-Aldrich, Gillingham, UK) within a glass microscopy chamber and left to set for 1 hour at 37 °C. 10 x RPMI (Sigma-Aldrich, Gillingham, UK) supplemented with 0-100 mmol/L sodium chloride (South Devon HealthCare, Torbay, UK) and 1:500 AF647-labelled wheat germ agglutinin (Invitrogen, Paisley, UK) was layered on top of the collagen matrix. The chamber was sealed and confocal microscopy undertaken. Cell measurements were performed using Imaris Software (Bitplane, La Jolla, USA).

Human monocyte derived macrophage assays

Leukocyte cones (NC24) were obtained from the National Blood Service (Cambridge, UK). Cell fractions were separated using Histopaque 1077 (Sigma-Aldrich, Gillingham, UK) and the monocyte layer retrieved. Cells were cultured in complete RPMI with 0.1 μ g/ml MCSF (Peprotech, London, UK) and were supplemented every 72 hr for 5-10 days. After stimulation with UPEC, supernatants were retrieved and IL6, TNF- α and IL8 measured with Quantikine ELISA kits (R and D, Abingdon, UK).

Bacterial killing assay

Human monocyte derived macrophages were prepared as detailed below, with or without 100 mmol/L sodium chloride (South Devon HealthCare, Torbay, UK) for the final 48 hours. Cells were incubated with opsonised UT189 (MOI 100) and fresh Optimem medium (Gibco, Paisley,

UK) for 45 minutes at 37°C with 5% CO₂. Cells were washed 3 times with PBS. Fresh OptiMem containing 100 µg/ml gentamicin (Gibco, Paisley, UK) was added and cells incubated for a further 15 (T0), 60 (T1) or 120 (T2) minutes. Cells were water lysed and plated out on LB agar in serial dilutions and incubated overnight (T0 and T2) and colonies counted using the aCOLyte-3 colony counter (Synbiosis, Cambridge, UK). Samples from T1 were lysed, resuspended in Live Cell Imaging Solution (Gibco, Paisley, UK) and stained using Live/Dead BacLight Bacterial Viability and Counting Kit (Gibco, Paisley, UK) as per manufacturer's protocol.

In vivo UTI experiment

Diabetes insipidus, CCL2 blockade or lithium treatment was induced in 6-8 week old female C57/BL6 or CD11c eYFP mice. Under isoflurane anesthesia (Baxter, Newbury, UK), the perineum was cleaned, the urethra catheterised using 0.28 x 0.60 mm polyethylene tubing (Instech Laboratories, PA, USA) and 100 µl of UPEC (OD₆₀₀ 0.5) instilled. Mice were sacrificed the following day and organs immediately perfused with sterile PBS. Kidney and spleen cell suspensions and blood were plated onto LB agar in serial dilutions and cultured overnight at 37°C without CO₂. CFUs were quantified using the aCOLyte-3 colony counter (Synbiosis, Cambridge, UK).

Quantification and statistical analysis

Statistical analyses

Statistical analyses were performed using Graphpad PRISM software (La Jolla, USA). Unless otherwise stated data are expressed as mean ± SEM. A two-tailed Student t-test was applied, unless otherwise indicated. Outliers were identified using the ROUT method within Graphpad PRISM.

All experiments were subject to at least three technical replicates per experimental parameter, and all data shown are representative of at least 3 individual experiments, unless where otherwise indicated. Biological replicates are shown as individual data points. * p<0.05, ** p<0.01, *** p<0.001, **** p<0.0001, NS p>0.05.

Meta-analysis of UTIs in sickle cell disease

A PubMed search from 2000-2015 using the terms "sickle cell disease AND [infection OR urine OR UTI OR urinary OR pyelonephritis]" was undertaken on 7th July 2015. All available abstracts were reviewed and all studies evaluating frequency of urinary tract infection (including pyelonephritis and asymptomatic bacteriuria) in patients with sickle cell disease (excluding

sickle cell trait) were included where the raw data were available. Data were analyzed using RevMan software Version 5.3 (Copenhagen, Denmark, The Cochrane Collaboration).

Microarray analysis

A previously published transcriptomic data set (Higgins et al., 2004) of n=4 paired human cortex and medulla samples from nephrectomy specimens was obtained from the Gene Expression Omnibus (GSE3931). RNA was extracted from macroscopically dissected cortex and medulla samples and gene expression assessed by microarray. The microarray data were analyzed with R (Gentleman et al., 2004) using Bioconductor packages Biobase, GEOquery and limma. Chemokines that were differentially expressed between the cortex and medulla were identified and a heatmap was generated using the gplots package within R.

Key resources table

REAGENT or RESOURCE	SOURCE	IDENTIFIER
Antibodies		
Live/ Dead Aqua 405	Invitrogen	L34957
Anti-human CD45 Monoclonal Antibody (2D1), PE	Thermo Fisher Scientific	Cat# 12-9459-42; RRID:AB_10718238
Anti-human CD45 Monoclonal Antibody (2D1), PerCP-Cy5.5	Thermo Fisher Scientific	Cat# 9045-9459-120; RRID:AB_11182108
Anti-human HLA-DR Monoclonal Antibody (L243), eFluor 450	Thermo Fisher Scientific	Cat# 48-9952-42; RRID:AB_1603291
Anti-human CD11c Monoclonal Antibody (3.9), PE-Cyanine7	Thermo Fisher Scientific	Cat# 25-0116-42; RRID:AB_1582274
Anti-human CX3CR1 Monoclonal Antibody (2A9-1), PE	Thermo Fisher Scientific	Cat# 12-6099-42; RRID:AB_10852707
Anti-human TNF alpha Monoclonal Antibody (MAb11), PE	Thermo Fisher Scientific	Cat# 12-7349-82; RRID:AB_466208
Anti-human IL-6 Monoclonal Antibody (MQ2-13A5), PE-Cyanine7	Thermo Fisher Scientific	Cat# 25-7069-42; RRID:AB_2573522
Anti-human CD206 (MMR) Monoclonal Antibody (19.2), Alexa Fluor 488	Thermo Fisher Scientific	Cat# 53-2069-42; RRID:AB_2574416
Anti-human CD11b Monoclonal Antibody (C67F154), Alexa Fluor 488	Thermo Fisher Scientific	Cat# 53-0196-82; RRID:AB_2637196
Anti-human CD64 (Fc gamma Receptor 1) Monoclonal Antibody (10.1), APC	Thermo Fisher Scientific	Cat# 17-0649-42; RRID:AB_10670630
Anti-human CD16 Monoclonal Antibody (eBioCB16 (CB16)), PE-Cyanine7	Thermo Fisher Scientific	Cat# 25-0168-42; RRID:AB_10714839
Anti-human CD209 (DC-SIGN) Monoclonal Antibody (eB-h209), PE	Thermo Fisher Scientific	Cat# 12-2099-42; RRID:AB_10853324
Anti-human CD172a (SIRP alpha) Monoclonal Antibody (15-414), APC	Thermo Fisher Scientific	Cat# 17-1729-42; RRID:AB_1944409
Anti-human CD8a Monoclonal Antibody (HIT8a), PE	Thermo Fisher Scientific	Cat# 12-0089-42; RRID:AB_10804039
Anti-human CD195 (CCR5) Monoclonal Antibody (NP-6G4), APC	Thermo Fisher Scientific	Cat# 17-1956-42; RRID:AB_2573178
Anti-human CD196 (CCR6) Monoclonal Antibody (R6H1), APC	Thermo Fisher Scientific	Cat# 17-1969-42; RRID:AB_10733388
Anti-human CD197 (CCR7) Monoclonal Antibody (3D12), PE-Cyanine7	Thermo Fisher Scientific	Cat# 25-1979-42; RRID:AB_2573422
Anti-human Brilliant Violet 650-conjugated anti-CD14 (clone M5E2)	Biolegend	Cat# 301836; RRID:AB_2563799
Anti-human APC-conjugated anti-CD192 (CCR2) (clone K036C2)	Biolegend	Cat# 357208; RRID:AB_2562239
Anti-human FITC conjugated anti-IL-8 (clone E8N1)	Biolegend	Cat# 511406; RRID:AB_893462
Anti-human Brilliant Violet 650-conjugated anti-CD15 (Clone W6D3)	Biolegend	Cat# 323034; RRID:AB_2563840
Anti- human APC conjugated anti-CD193 (CCR3) (clone 5E8)	Biolegend	Cat# 310708; RRID:AB_2228976
Anti-human PE conjugated anti-CD1a (clone HI149)	Miltenyi Biotech	Cat# 130-097-868; RRID:AB_2656020
Anti-human PE conjugated anti-CD1c (BDCA-1)(clone AD5-8E7)	Miltenyi Biotech	Cat# 130-090-508; RRID:AB_244315

Anti-human Alexa Fluor 700-conjugated anti-CD3 (clone UCHT1)	Biolegend	Cat# 300424; RRID:AB_493741
Anti-human Alexa Fluor 700-conjugated anti-CD15 (clone W6D3)	Biolegend	Cat# 323026; RRID:AB_2561427
Anti-human Alexa Fluor 700-conjugated anti-CD19 (clone HIB19)	Biolegend	Cat# 302226; RRID:AB_493751
Anti-human APC conjugated anti-CD68 (clone Y1182A)	Biolegend	Cat# 137008; RRID:AB_10575300
Anti-mouse APC conjugated anti-CD191 (CCR1) (clone 53504)	Biolegend	Cat# 362908; RRID:AB_2563919
Anti-human unconjugated rabbit NFAT5 polyclonal antibody	AbCam	Cat# ab172506
Anti-human NFAT5 polyclonal antibody (for Western blot)	Thermo Fisher Scientific	Cat# PA1-023; RRID:AB_2152617
Anti-human CCL2 (MCP-1) antibody (clone EP1361)	AbCam	Cat# ab151538;
Anti-human CX3CL1 antibody	AbCam	Cat# ab25088; RRID:AB_4486
Anti-human Langerin/CD207 Phycoerythrin MAb (Clone 343828)	R and D Systems	Cat# FAB2088P; RRID:AB_2074215
Anti-mouse CD45.2 Monoclonal Antibody (clone 104), APC-eFluor 780	Thermo Fisher Scientific	Cat# 47-0454-82; RRID:AB_1272175
Anti-mouse CD3 Monoclonal Antibody (clone 17A2), eFluor 450	Thermo Fisher Scientific	Cat# 48-0032-82; RRID:AB_1272193
Anti-mouse CD19 (clone eBio 1D3), eFluor 450	Thermo Fisher Scientific	Cat# 48-0193-82; RRID:AB_2043815
Anti-mouse Ly-6G (Gr-1) (clone RB6-8C5), eFluor 450	Thermo Fisher Scientific	Cat# 48-5931-82; RRID:AB_1548788
Anti-mouse CD11b Monoclonal antibody(clone M1/70), PerCP-Cyanine5.5	Thermo Fisher Scientific	Cat# 45-0112-82; RRID:AB_953558
Anti-mouse CD11c Monoclonal Antibody (clone N418), PE-Cyanine7	Thermo Fisher Scientific	Cat# 25-0114-82; RRID:AB_469590
Anti-mouse MHC Class II (I-A/I-E) Monoclonal Antibody (clone M5/114.15.2), Alexa Fluor 700)	Thermo Fisher Scientific	Cat# 56-5321-82; RRID:AB_494009
Anti-mouse F4/80 Monoclonal Antibody (clone BM8), FITC	Thermo Fisher Scientific	Cat# 11-4801-82; RRID:AB_2637191
Anti-mouse F4/80 Monoclonal Antibody (clone BM8), APC	Thermo Fisher Scientific	Cat# 17-4801-82; RRID:AB_469452
Anti-mouse IL-6 Monoclonal Antibody (clone MP5-20F3), PE	Thermo Fisher Scientific	Cat# 12-7061-82; RRID:AB_466165
Anti-mouse TNF alpha Monoclonal Antibody (clone MP6-XT22), PE	Thermo Fisher Scientific	Cat# 12-7321-82; RRID:AB_466199
Anti-mouse Ki-67 Monoclonal Antibody (clone SolA15), PE	Thermo Fisher Scientific	Cat# 12-5698-82; RRID:AB_11150954
Anti-mouse CCL2 (MCP-1) Monoclonal Antibody (clone 2H5)	Thermo Fisher Scientific	Cat# 16-7096-85; RRID:AB_469221
Rabbit anti-mouse biotinylated anti-CXCL2 (Clone AAM48B)	Biorad	Cat# AAM48B; RRID:AB_2230059
Anti-mouse CX3CR1 (clone SA011F11), Brilliant Violet 650	Biolegend	Cat# 149033; RRID:AB_2565999
Brilliant Violet-605 Streptavidin	Biolegend	Cat# 405229
Anti-mouse/human CD11b (Clone M1.70), Alexa fluor 488	Biolegend	Cat# 101217; RRID:AB_389305
FITC conjugated anti-E. coli.	AbCam	Cat# ab30522; RRID:AB_732219

Rat Anti-Mouse CD45 (clone 30-F11), BUV 395	BD Biosciences	Cat# 564279; RRID:AB_2651134
beta Actin loading control Monoclonal Antibody (clone BA3R)	Thermo Fisher Scientific	Cat# MA5-15739; RRID:AB_10979409
Donkey anti-Rabbit IgG Secondary Antibody, Alexa Fluor 488	Thermo Fisher Scientific	Cat# R37118; RRID:AB_2556546
AF568-conjugated phalloidin	Thermo Fisher Scientific	Cat# A12380
AF488 conjugated polyclonal rabbit anti-GFP	Thermo Fisher Scientific	Cat# A21311
Goat anti-Rabbit IgG (H+L) Secondary Antibody, Pacific Blue	Invitrogen	Cat# P-10994; RRID:AB_2539814
Anti-rabbit IgG (H+L) (DyLight™ 680 Conjugate)	Cell Signaling Technology	Cat# 5366
Anti-rabbit IgG (H+L) (DyLight™ 800 4X PEG Conjugate)	Cell Signaling Technology	Cat# 5151
Bacterial and Virus Strains		
Uropathogenic E. coli (UPEC, UT189)	a gift from S. Hultgren (Hung et al., 2009)	
Biological Samples		
Human kidney samples (ethical approval REC12/EE/0446)	NHSBT	
Human whole blood samples (ethical approval REC08/H0308/176)	National Blood Service	Cat# Leukocyte cone NC24
Chemicals, Peptides, and Recombinant Proteins		
Recombinant human CX3CL1	Life Technologies	Cat# 10636H08H50
Recombinant human CCL2	R & D Systems	Cat# 279-MC-050;
0-120 mmol/L sodium chloride	South Devon Healthcare, Torbay	Cat# Sodium Chloride 30% w/v Concentrate
0-200 mOsmol/kg 20% mannitol	Baxter	Cat# mannitol
Demeclocycline	LKT Laboratories	Cat# D1748
Tolvaptan	Sigma-Aldrich	Cat# T7455-Tolvaptan
CCL2 (MCP-1) Monoclonal Antibody (clone 2H5)	Thermo Fisher Scientific	Cat# 14-7096-81; RRID:AB_468430
lithium chloride	Thermo Fisher Scientific	Cat# AM9480
Tamoxifen	Sigma-Aldrich	Cat# T5648 - Tamoxifen
100 ng/ml E. coli lipopolysaccharide	Sigma-Aldrich	Cat# L2630
p38 inhibitor SB203580	Cell signaling technology	Cat# SB203580 5633
Bortezomib (PS-341) proteasome inhibitor	SelleckChem	Cat# S1013
Critical Commercial Assays		
FoxP3 intracellular staining kit	eBioscience	Cat# 00-5521-00
CD11c bead separation	BD Biosciences	Cat# 130-097-059
MACS separation using LS columns	Miltenyi Botech	Cat# 130-042-401
Complementary DNA synthesis; High capacity RNA to cDNA	Life Technologies	Cat# 4387406
NFAT5 siRNA knockdown (using Lipofectamine and silencer select siRNA)	Thermo Fisher Scientific	Lipofectamine Cat# 18324012; siRNA Cat# AM16708

Deposited Data		
Paired human cortex and medulla kidney samples	Higgins et al., 2004	Gene Expression Omnibus (GSE3931)
Experimental Models: Cell Lines		
Renal tubular epithelial cells (HK2 cells)	ATCC	Cat# CRL-2190; RRID:CVCL_0302
Experimental Models: Organisms/Strains		
Mouse: Wild-type C57BL/6	Jackson Laboratories	Stock No: 000664
Mouse: UBI-GFP-BL/6 mice. Strain ID: C57BL/6-Tg(UBC-GFP)30Scha/J	Jackson Laboratories	Stock No: 004353
Mouse: CD11c EYFP Strain ID: B6.Cg-Tg(Itgax-Venus)1Mnz/J	Gift from M. Nussenzweig	Stock No: 008829 (Jackson Laboratories)
Mouse: <i>Ccr2</i> ^{-/-} Strain ID: B6.129S4-Ccr2tm1lfc/J	(Boring et al., 1997) Gift from Callum Bain and Simon Jenkins	Stock No: 004999 (Jackson Laboratories)
Mouse: <i>Nfat5</i> ^{fl/fl}	(Kuper et al., 2014) gifted by Christoph Kuper and Wolfgang Neuhofer	
Mouse: <i>Nfat5</i> ^{fl/fl} <i>Ert2-Cre</i>	(Kuper et al., 2014) gifted by Christoph Kuper and Wolfgang Neuhofer	
Oligonucleotides		
RT-PCR GAPDH	Life Technologies	Human Assay ID; Hs99999905_m1 Mouse Assay ID; Mm99999915_g1
RT-PCR Human GUSB	Life Technologies	Assay ID; Hs9999908_m1
RT-PCR HPRT	Life Technologies	Human Assay ID; Hs99999909_m1 Mouse Assay ID; Mm01545399_m1
RT-PCR NFAT5	Life Technologies	Human Assay ID; Hs00232437_m1 Mouse Assay ID; Mm00467257_m1
RT-PCR CCL2	Life Technologies	Human Assay ID; Hs00234140_m1 Mouse Assay ID; Mm00441242_m1
RT-PCR CX3CL1	Life Technologies	Human Assay ID; Hs00171086_m1 Mouse Assay ID; Mm00436454_m1
Software and Algorithms		
Flowjo software	Treestar	
Imaris	Bitplane	
Fiji/ ImageJ	ImageJ	
GraphPad PRISM	GraphPad PRISM	
R; Bioconductor packages Biobase, GEOquery and limma	Gentleman et al., 2004	

Other		
eFluor 670; used for labelling UPEC	Invitrogen	Cat# 65-0840-85
Human Myeloperoxidase Quantikine ELISA Kit	R & D Systems	Cat# DMYE00B
Human CX3CL1/Fractalkine Quantikine ELISA Kit	R & D Systems	Cat# DCX310
Human CCL2/MCP-1 Quantikine ELISA Kit	R & D Systems	Cat# DCP00
Human IL-6 Quantikine ELISA Kit	R & D Systems	Cat# D6050
Human TNF-alpha Quantikine ELISA Kit	R & D Systems	Cat# DTA00C
Human IL-8/CXCL8 Quantikine ELISA Kit	R & D Systems	Cat# D8000C

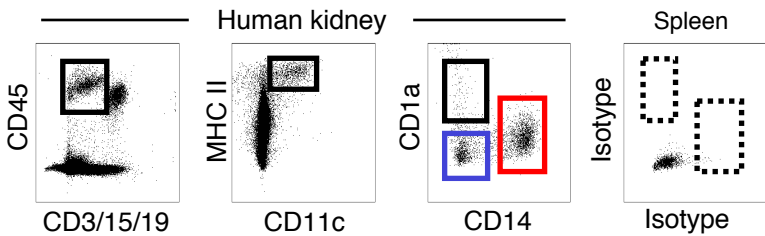
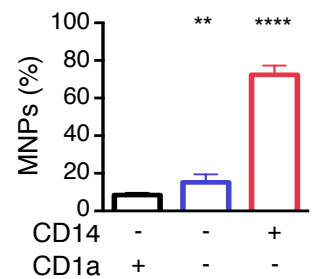
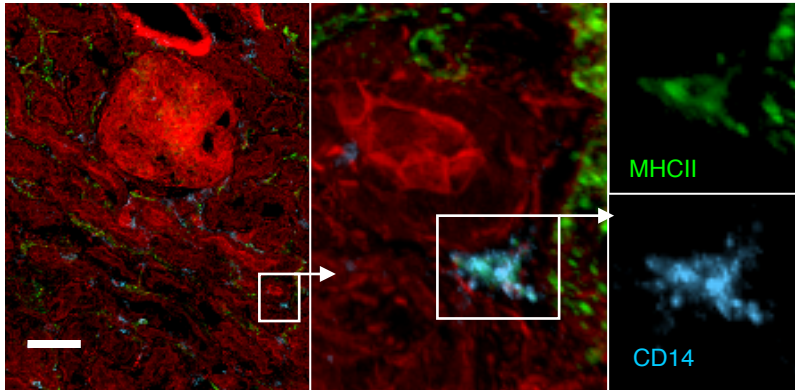
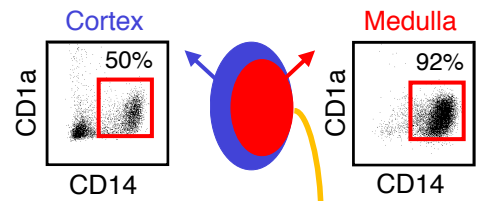
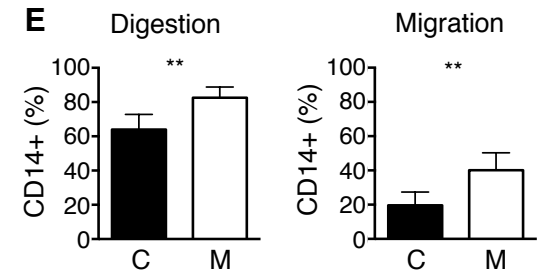
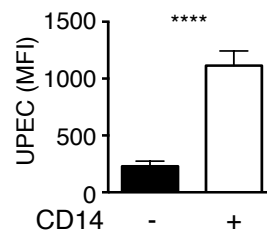
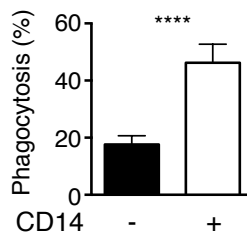
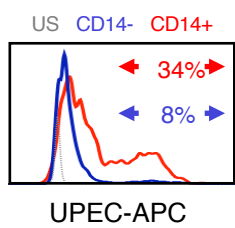
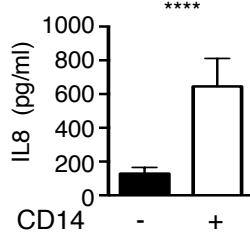
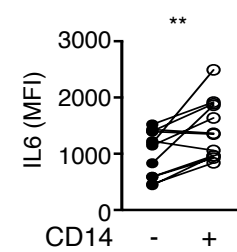
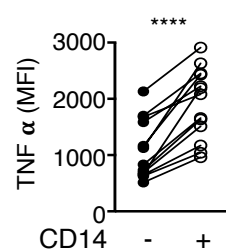
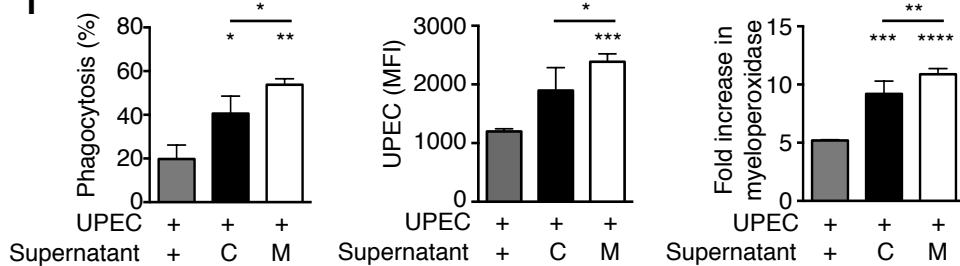
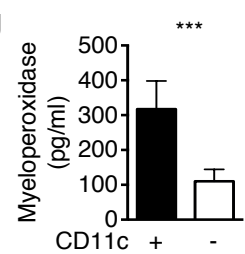
Figure 1**A****B****C****D****E****F** Human renal MNPs**G****H****I****J**

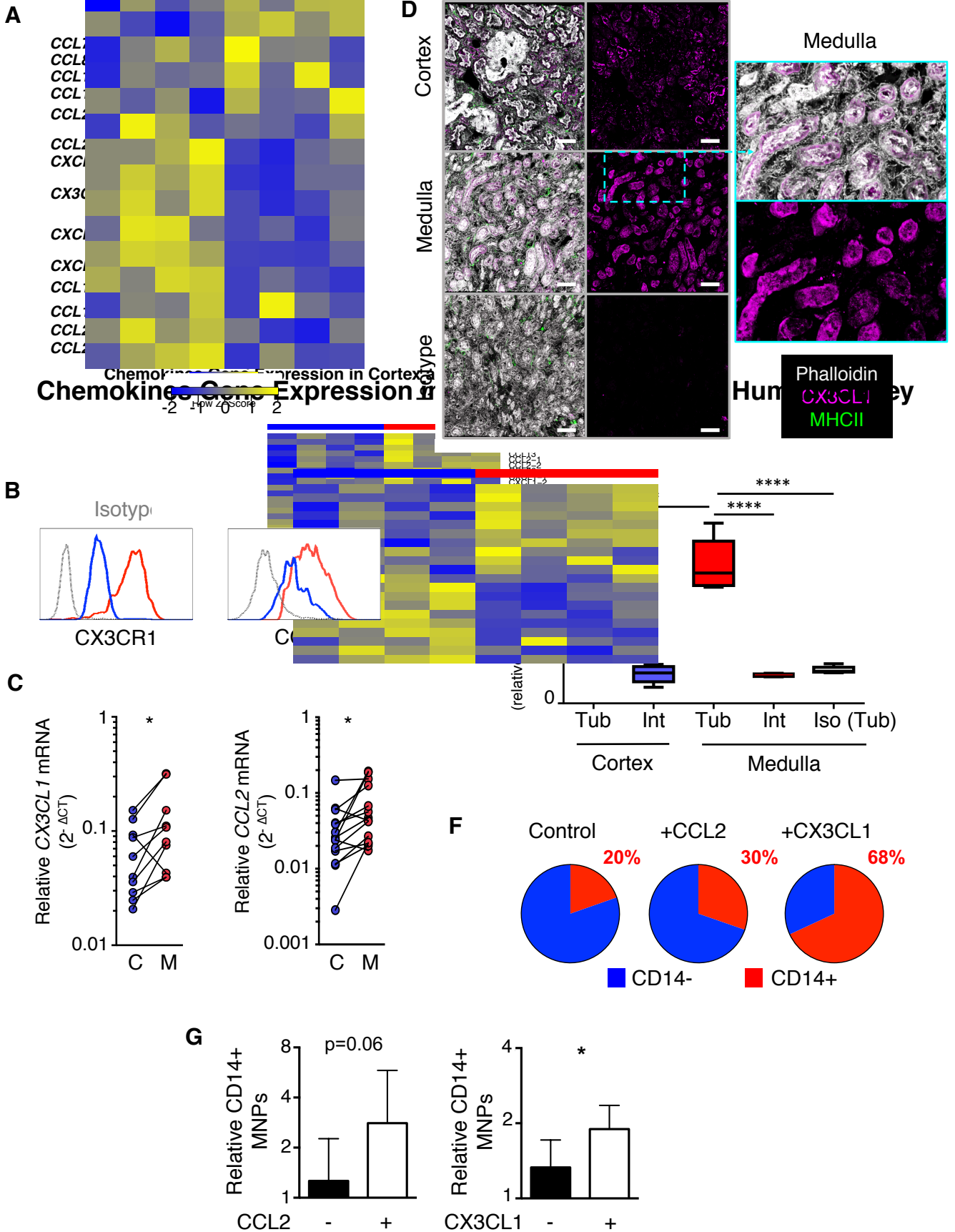
Figure 2

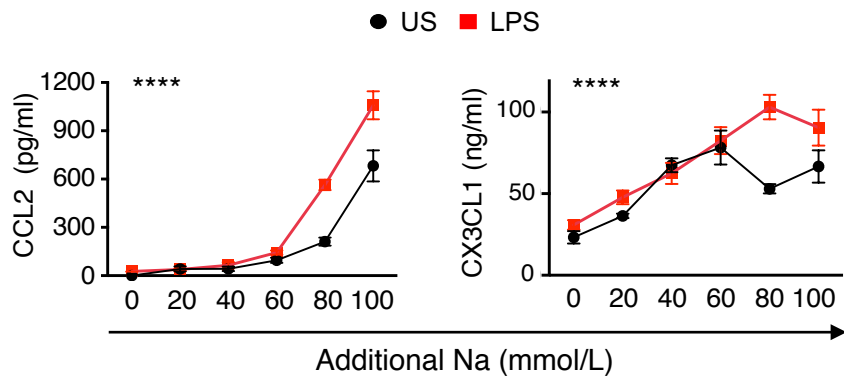
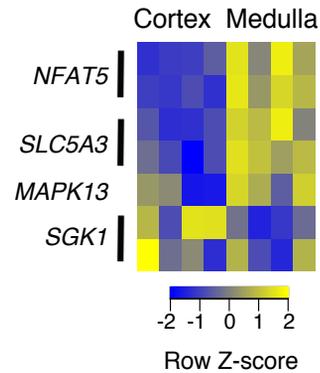
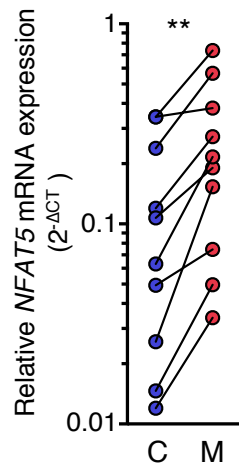
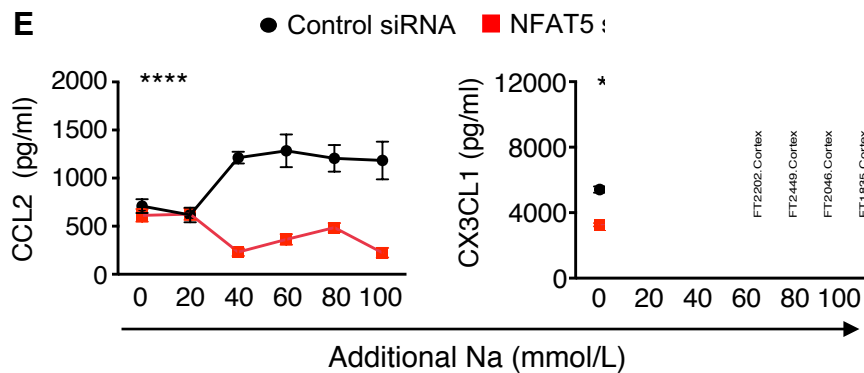
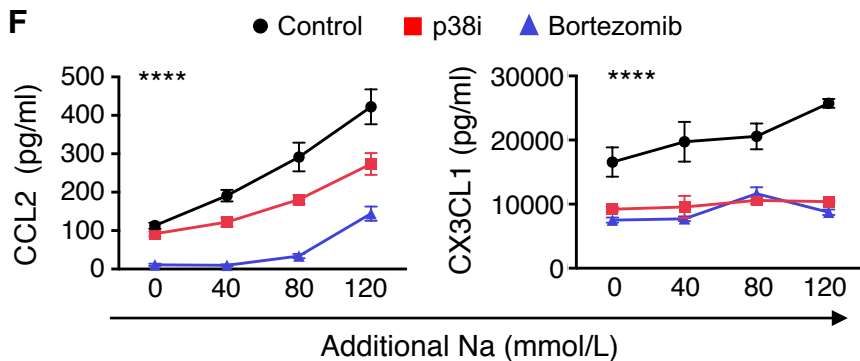
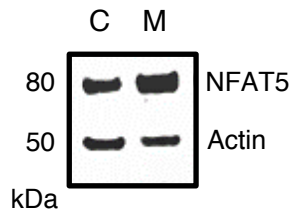
Figure 3**A****B****C****E****F****D**

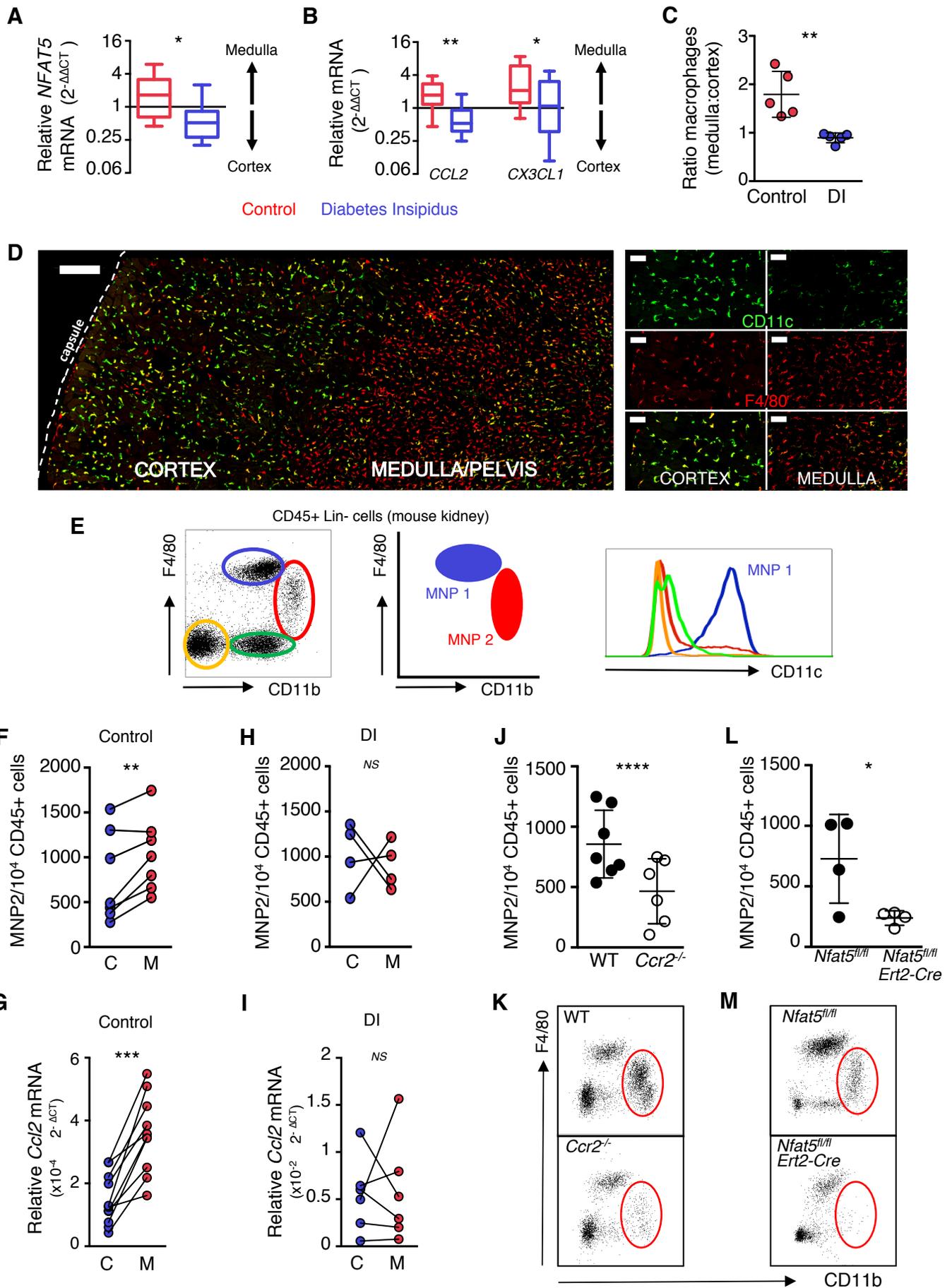
Figure 4

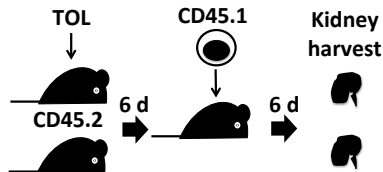
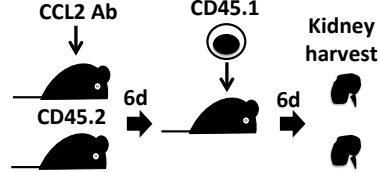
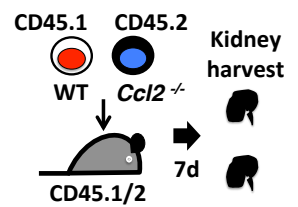
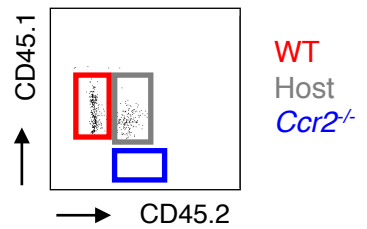
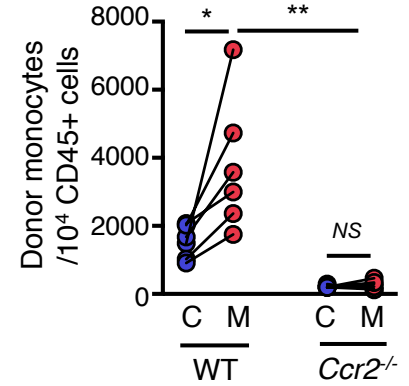
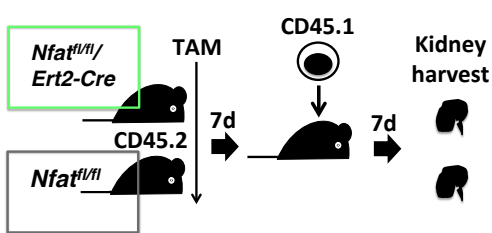
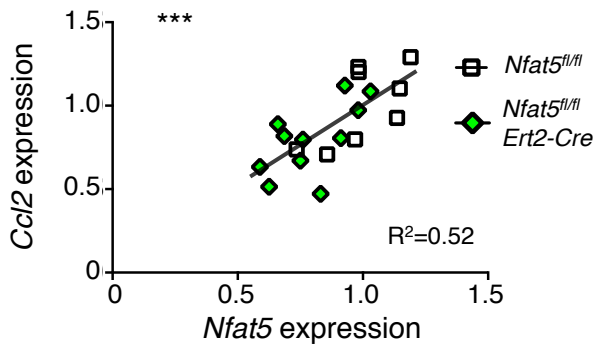
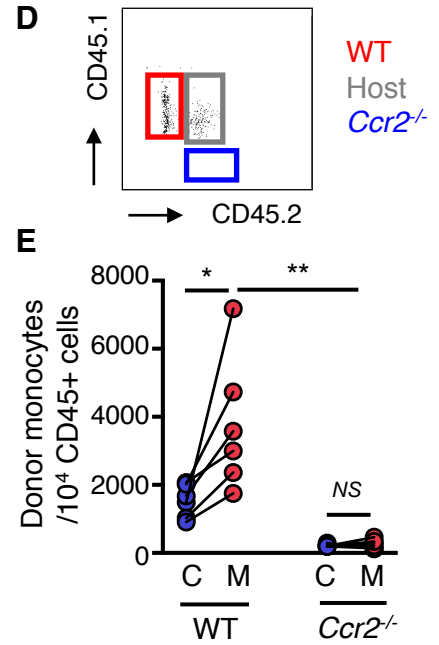
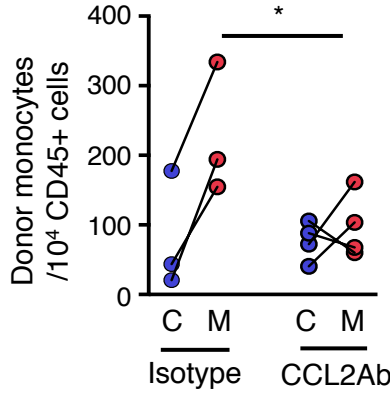
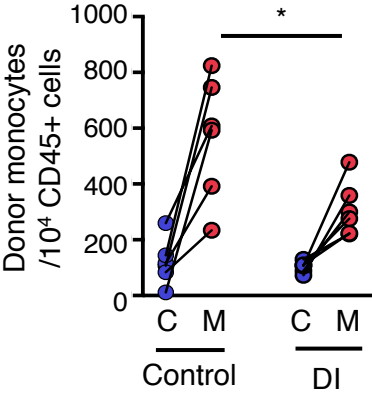
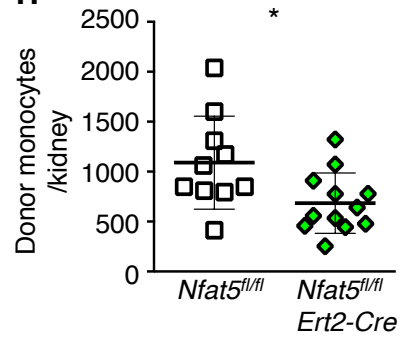
Figure 5**A****B****C****D****E****F****G****H**

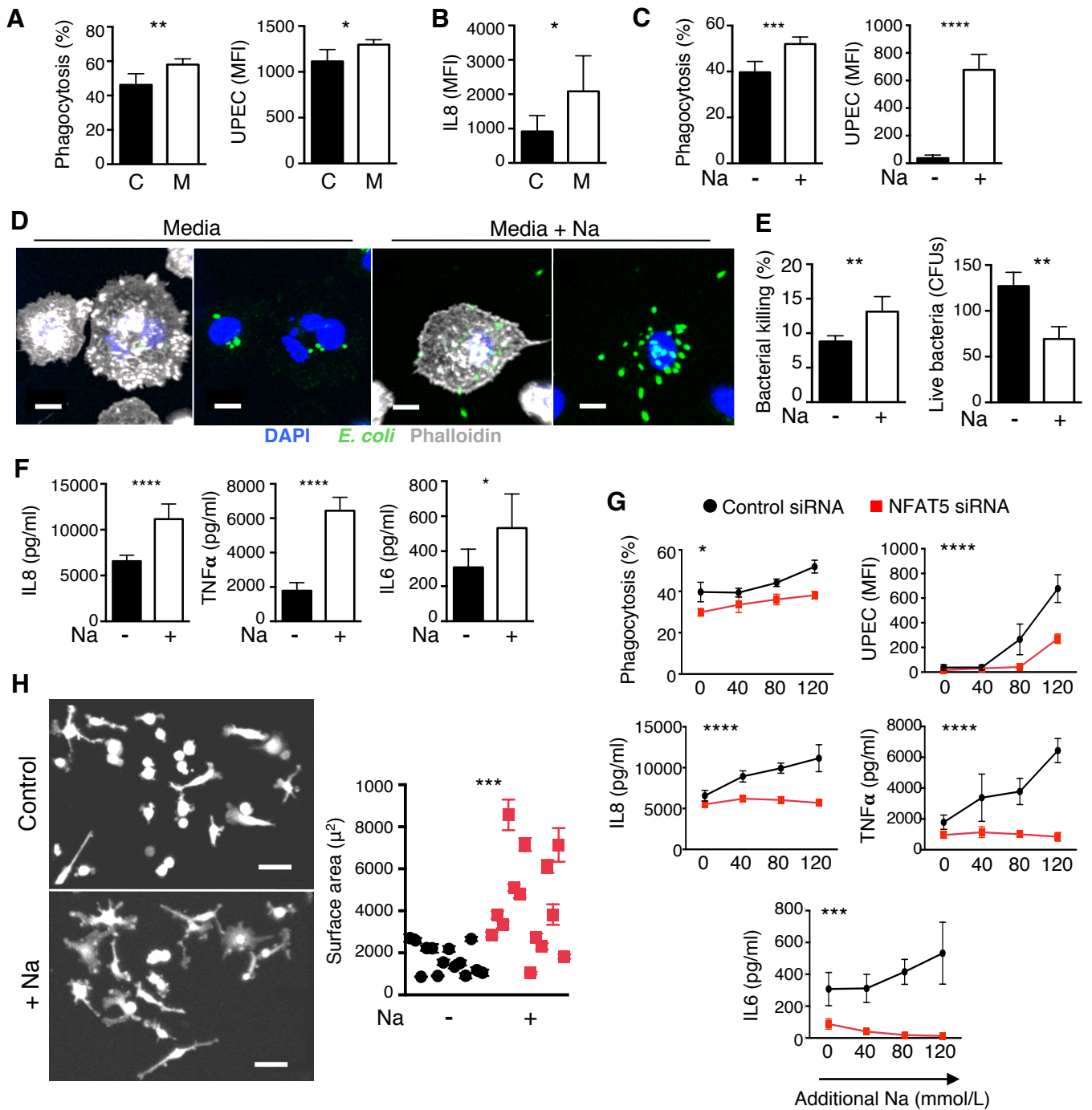
Figure 6

Figure 7

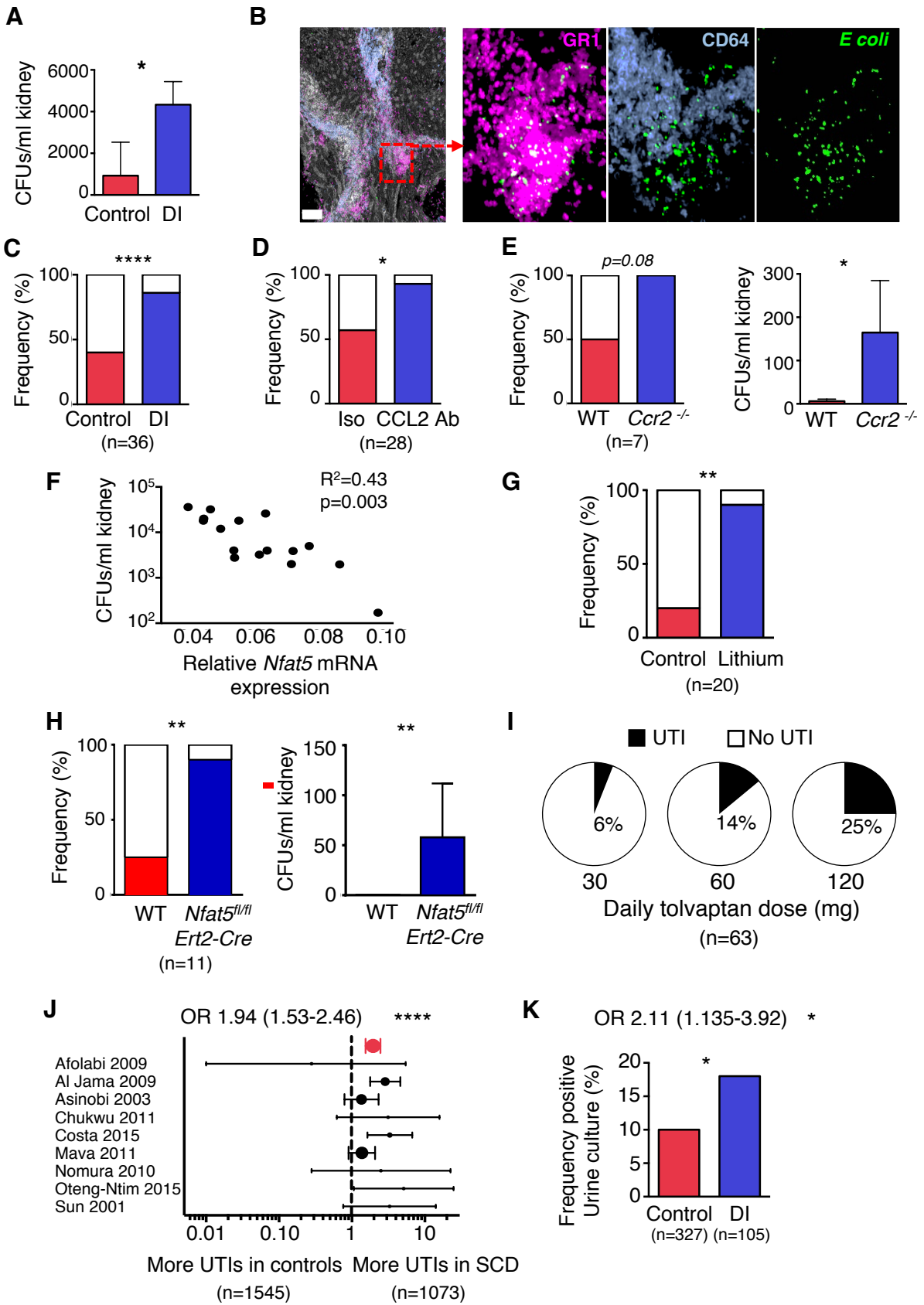
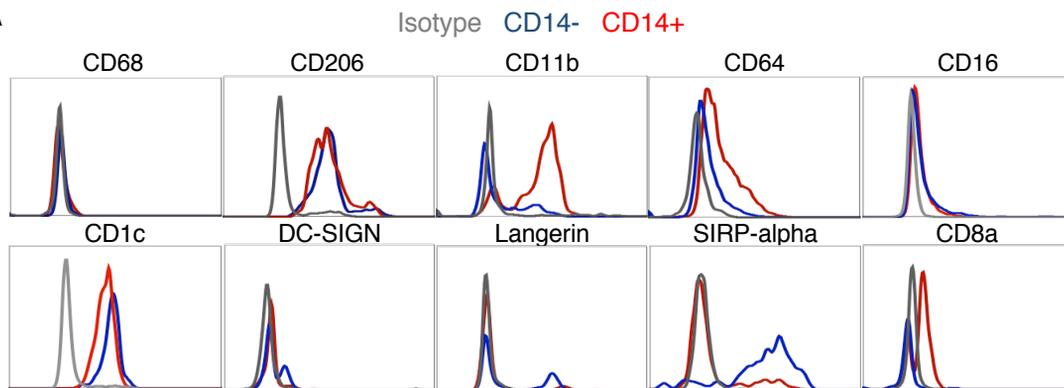
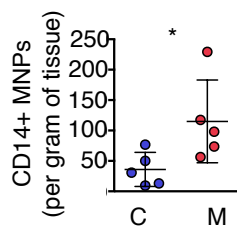


Figure S1, related to Figure 1

S1A



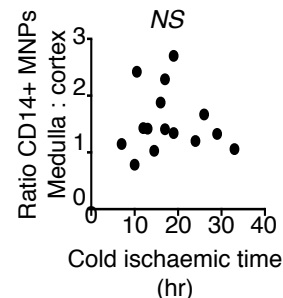
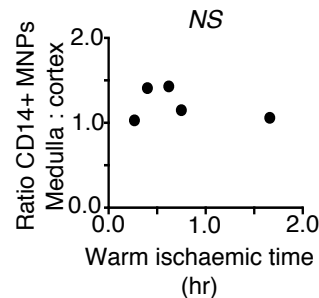
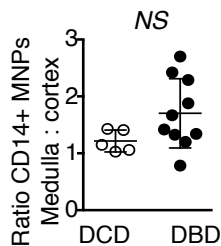
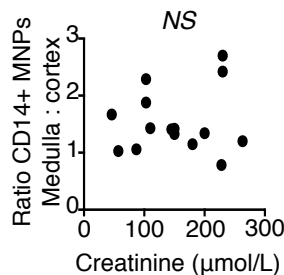
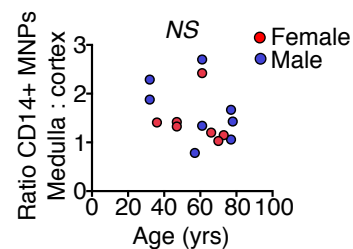
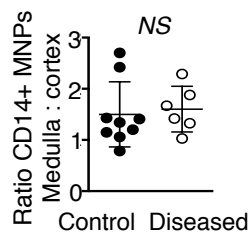
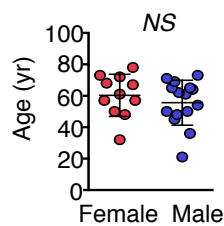
S1B



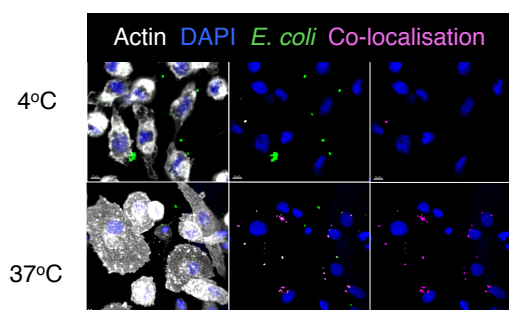
S1C

Reason declined	N (%)
Surgical/anatomical	18 (35.2)
?Malignancy	9 (17.6)
Perfusion	8 (15.7)
Biopsy	5 (9.8)
Infection	4 (7.8)
Operational	4 (7.8)
Renal function	1 (2)
Unknown	1 (2)

Cause of death	N (%)
Cerebral event	26 (51.0)
Cardiorespiratory	17 (33.3)
Trauma	4 (7.8)
Abdominal	3 (5.9)
Other	1 (2)



S1D



S1E

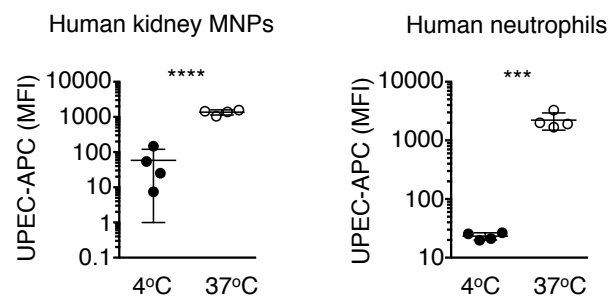
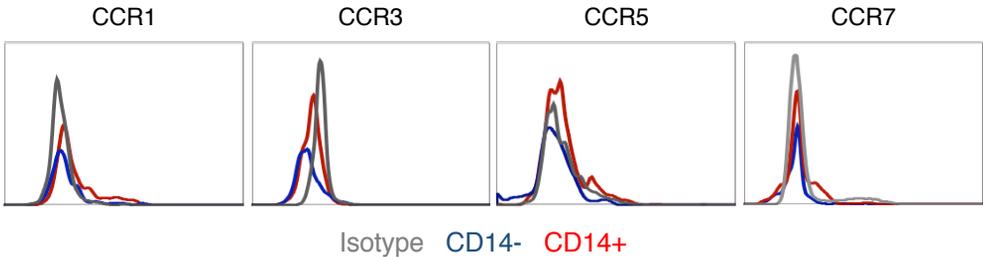


Figure S2, related to Figure 2

S2A



S2B

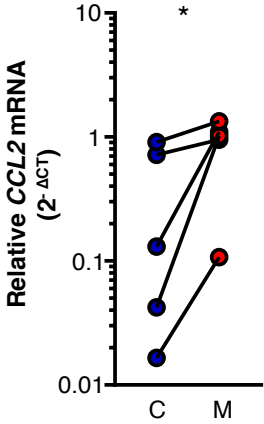
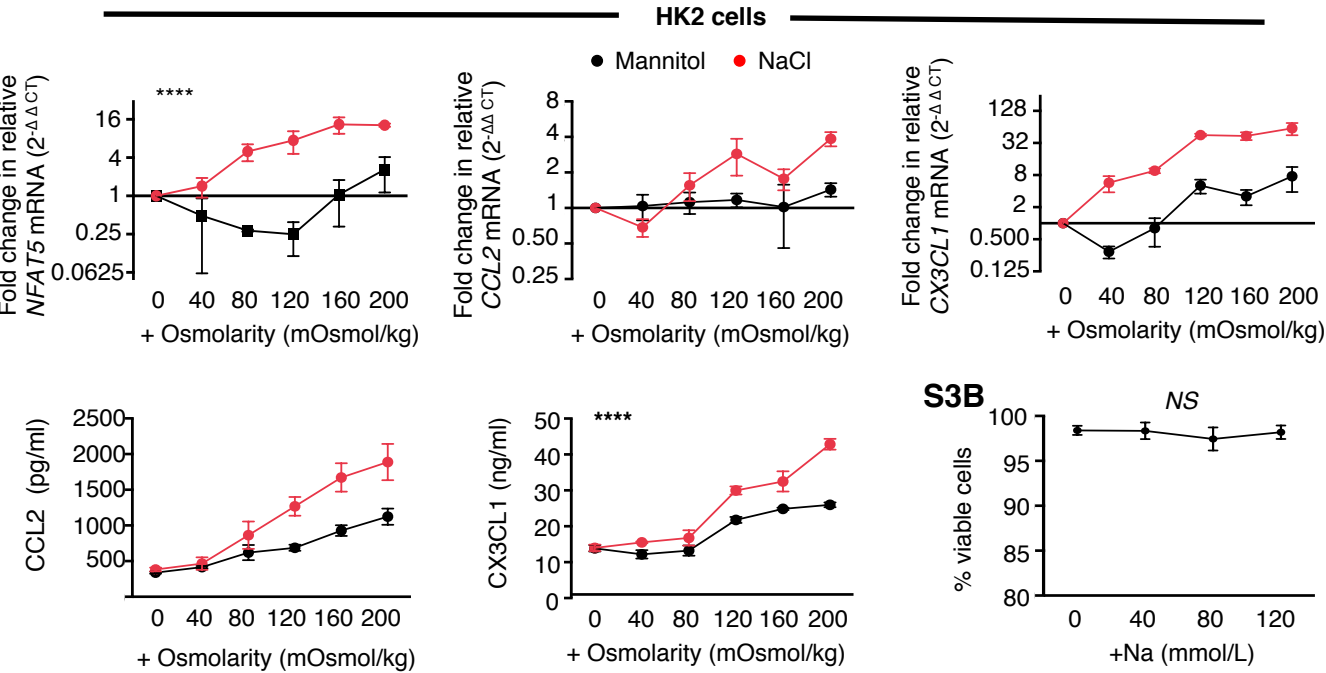
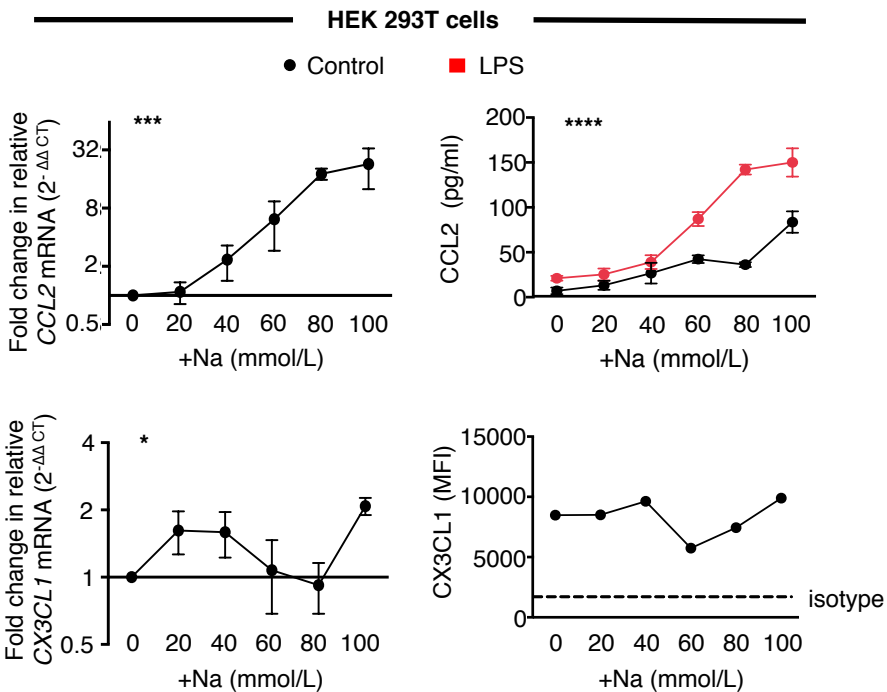


Figure S3, related to Figure 3

S3A



S3C



S3D

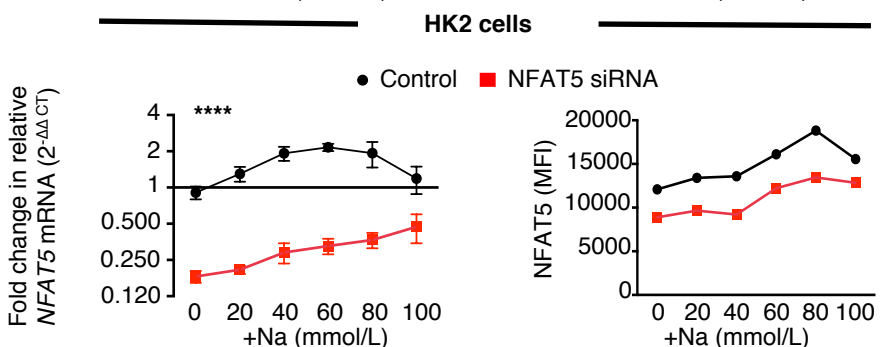
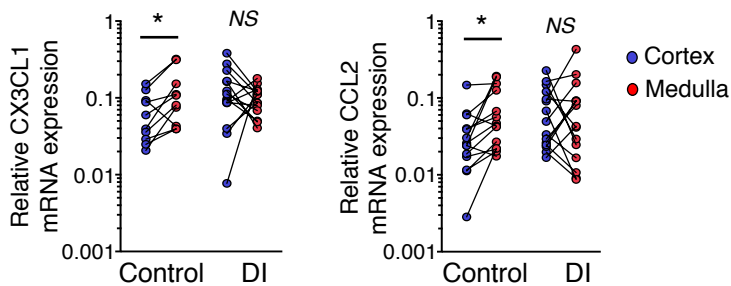
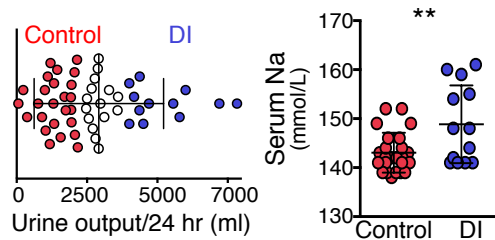


Figure S4, related to Figure 4

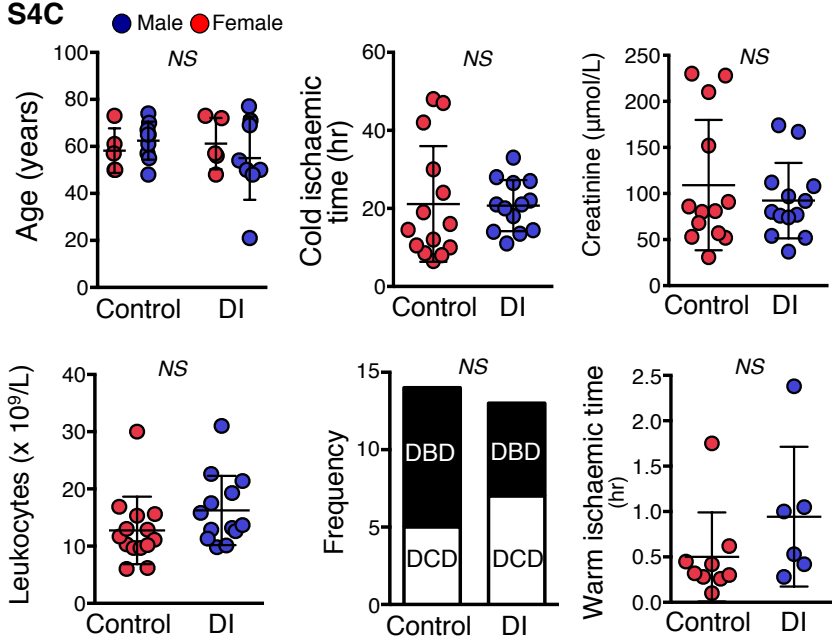
S4B



S4A



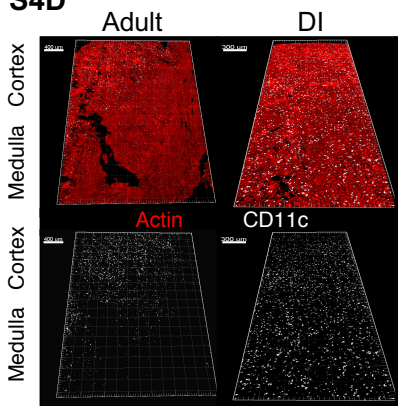
S4C



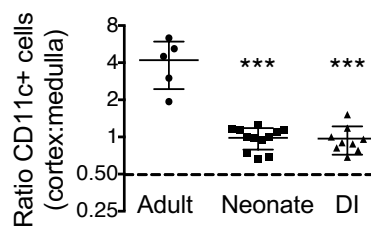
Reason declined	Control (N=14)	DI (N=13)
Surgical/anatomical	4	6
?Malignancy	4	1
Perfusion	3	2
Biopsy	1	2
Infection	0	1
Logistical	2	1
Cause of Death		
Cerebral event	7	9
Cardiorespiratory	7	3
Trauma	0	1
Other factors		
Corticosteroids	3	5
Active infection	5	4

All non-significant

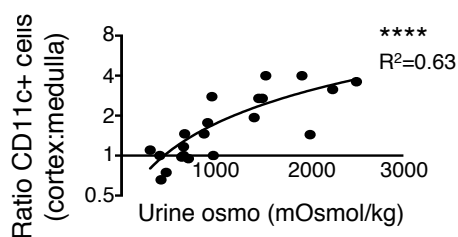
S4D



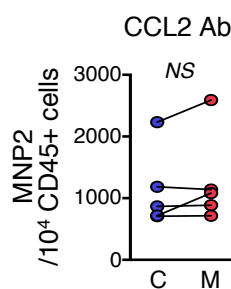
S4E



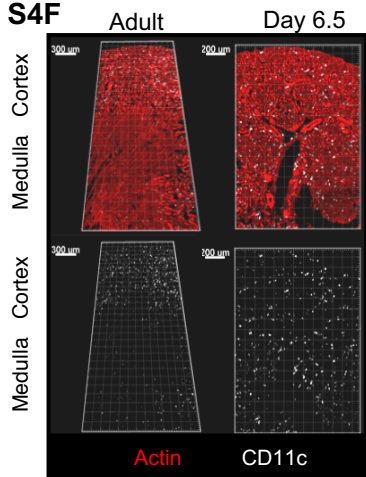
S4H



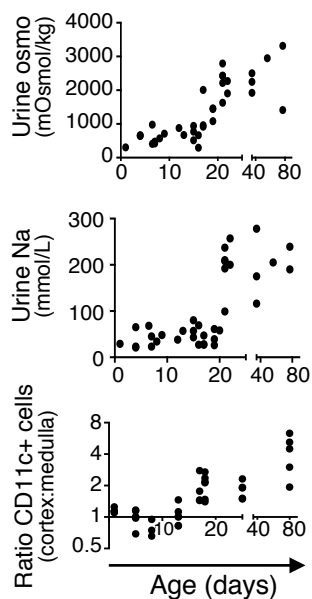
S4I



S4F



S4G



S4J

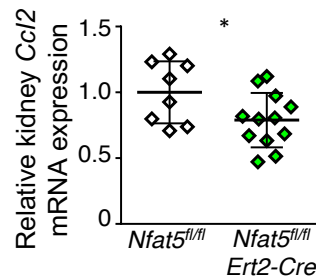
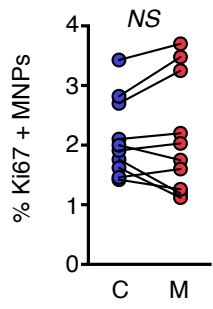


Figure S5, related to Figure 5

S5A



S5B

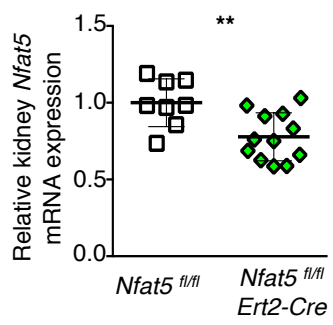
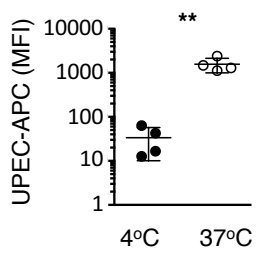
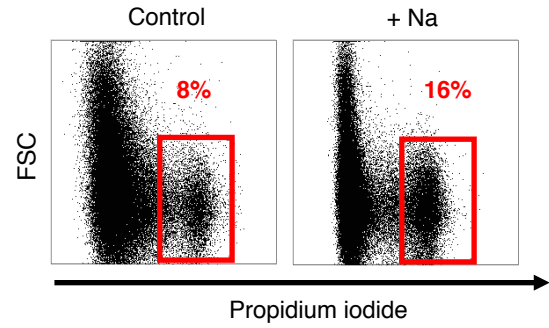


Figure S6, related to Figure 6

S6A



S6B



S6C

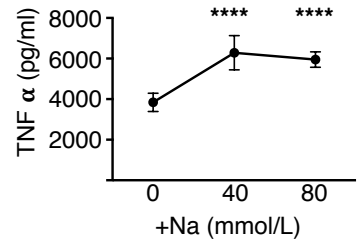
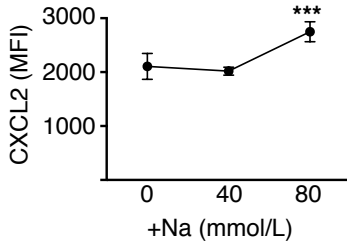
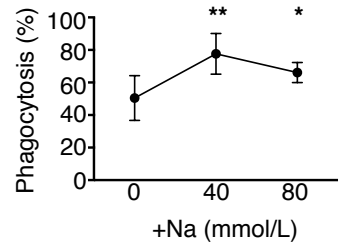
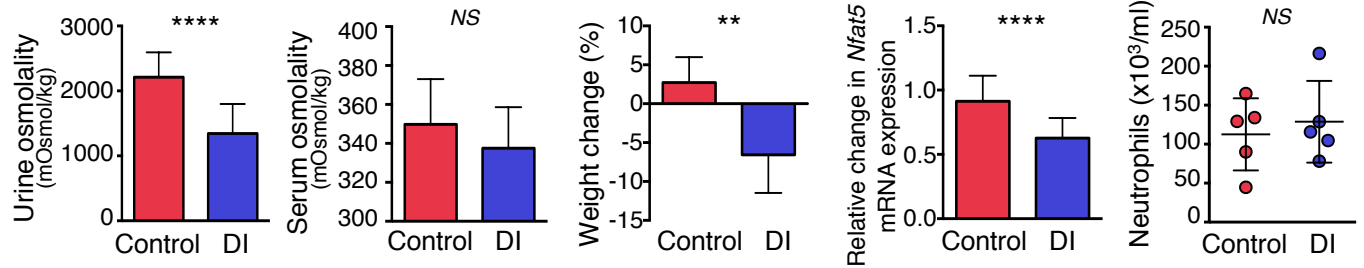
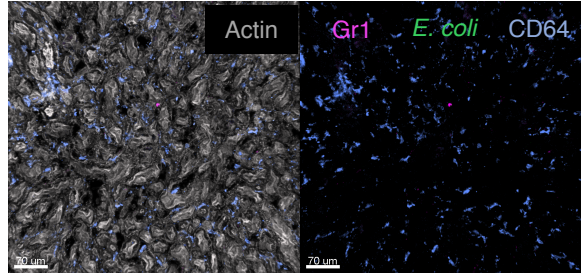
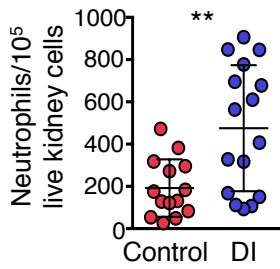


Figure S7, related to Figure 7

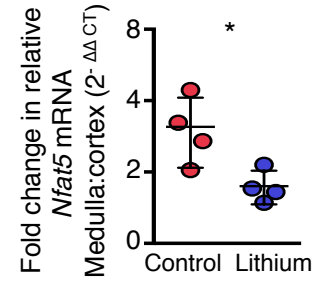
S7A



S7B



S7C

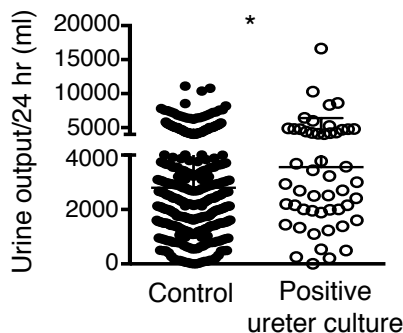


S7D

Sickle Cell Disease Meta-Analysis Bibliography

- Afolabi BB, Iwuala NC, Iwuala IC, Ogedengbe OK. Morbidity and mortality in sickle cell pregnancies in Lagos, Nigeria: a case control study. *Journal of obstetrics and gynaecology : the journal of the Institute of Obstetrics and Gynaecology* 2009;29:104-6.
- Al Jama FE, Gasem T, Burshaid S, Rahman J, Al Suleiman SA, Rahman MS. Pregnancy outcome in patients with homozygous sickle cell disease in a university hospital, Eastern Saudi Arabia. *Archives of gynecology and obstetrics* 2009;280:793-7.
- Asinobi AO, Fatunde OJ, Brown BJ, Osinusi K, Fasina NA. Urinary tract infection in febrile children with sickle cell anaemia in Ibadan, Nigeria. *Annals of tropical paediatrics* 2003;23:129-34.
- Chukwu BF, Okafor HU, Ikefuna AN. Asymptomatic bacteriuria in children with sickle cell anemia at The University of Nigeria teaching hospital, Enugu, South East, Nigeria. *Italian journal of pediatrics* 2011;37:45.
- Costa VM, Viana MB, Aguiar RA. Pregnancy in patients with sickle cell disease: maternal and perinatal outcomes. *The journal of maternal-fetal & neonatal medicine : the official journal of the European Association of Perinatal Medicine, the Federation of Asia and Oceania Perinatal Societies, the International Society of Perinatal Obstet* 2015;28:685-9.
- Mava Y, Ambe JP, Bello M, Watila I, Nottidge VA. Urinary tract infection in febrile children with sickle cell anaemia. *West African journal of medicine* 2011;30:268-72.
- Nomura RM, Igai AM, Tosta K, da Fonseca GH, Gualandro SF, Zugaib M. [Maternal and perinatal outcomes in pregnancies complicated by sickle cell diseases]. *Revista brasileira de ginecologia e obstetrica : revista da Federacao Brasileira das Sociedades de Ginecologia e Obstetrica* 2010;32:405-11.
- Oteng-Ntim E, Ayensah B, Knight M, Howard J. Pregnancy outcome in patients with sickle cell disease in the UK--a national cohort study comparing sickle cell anaemia (HbSS) with HbSC disease. *British journal of haematology* 2015;169:129-37.
- Sun PM, Wilburn W, Raynor BD, Jamieson D. Sickle cell disease in pregnancy: twenty years of experience at Grady Memorial Hospital, Atlanta, Georgia. *American journal of obstetrics and gynecology* 2001;184:1127-30.

S7E



Methodology for donor ureter study

Index cases	Control cases
N=1109 donor ureter pathology reports Cambridge 2007-2014	All deceased donor kidney transplants Cambridge 2007-14
N=90 positive donor ureter reports	Donor data available for N=742
Excluded: duplicate donors or >1 organism, living donor, incomplete data or likely contaminant	Excluded: incomplete data or positive donor ureter culture
Donor information for N=50 positive ureter cultures evaluated	Donor information for N=382 control cases evaluated
N=23 DBD N= 27 DCD	N=201 DBD N= 181 DCD